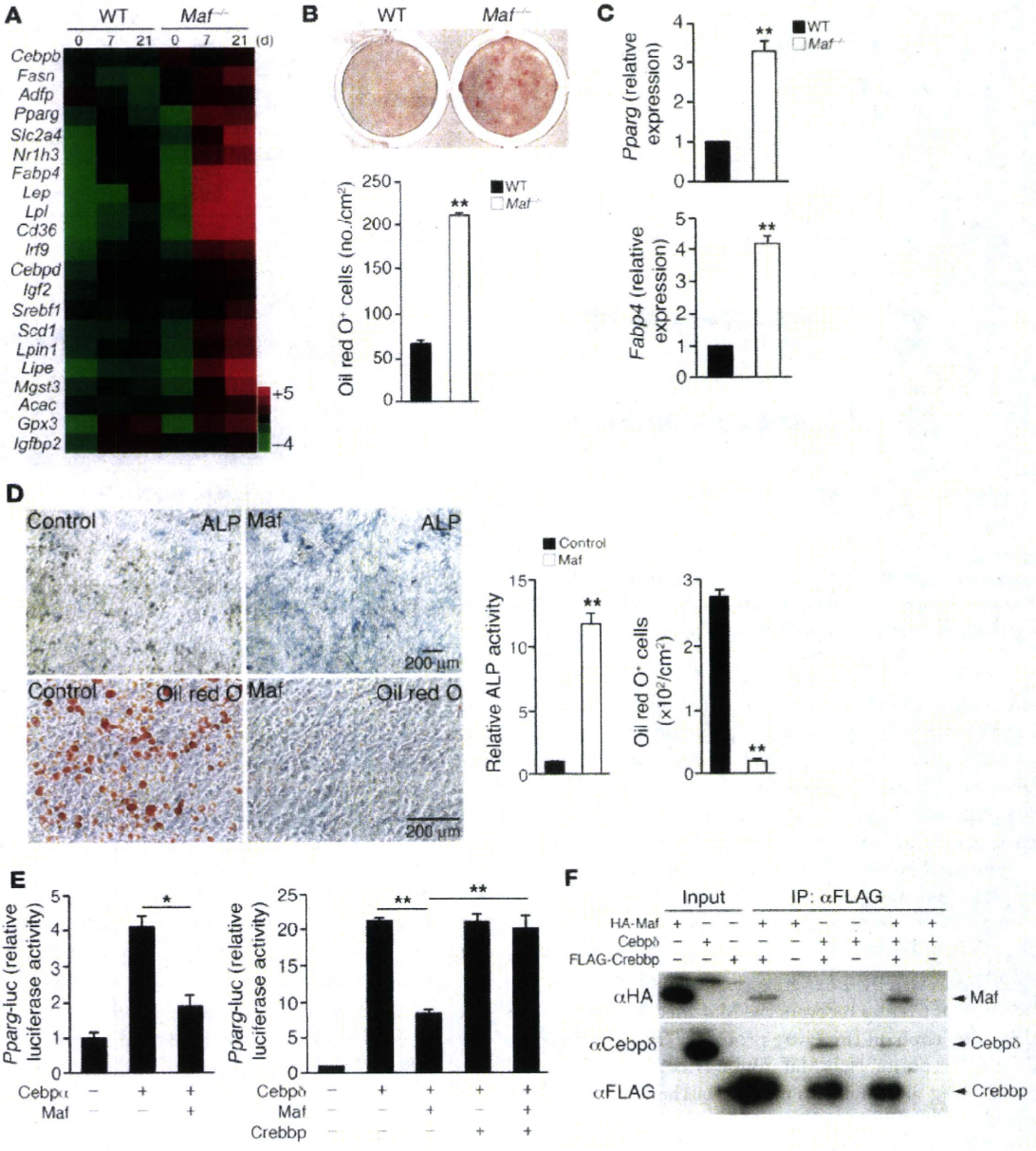

Figure 4

Maf inhibition of adipocyte differentiation by suppressing Cebpδ/α-mediated induction of *Pparg*. (**A**) mRNA expression of adipocyte-specific genes in WT and *Maf*$^{-/-}$ calvarial cells cultured with osteogenic medium (GeneChip analysis). (**B**) Adipocyte formation in WT and *Maf*$^{-/-}$ calvarial cells cultured with osteogenic medium (oil red O staining). (**C**) Expression of *Pparg* and *Fabp4* in WT and *Maf*$^{-/-}$ calvarial cells cultured with osteogenic medium (real-time RT-PCR analysis). (**D**) Effect of Maf overexpression on adipocyte and osteoblast differentiation of C3H10T1/2 cells. Scale bar: 200 μm. (**E**) Effect of Crebbp overexpression on Maf-mediated inhibition of Cebpδ activation of the *Pparg* promoter. (**F**) Inhibition of interaction between Cebpδ and Crebbp by Maf. $^{*}P < 0.05$; $^{**}P < 0.01$.

Furthermore, to gain mechanistic insight into the downregulation of *Maf* by ROS, we focused on the regulation of *Maf* by Trp53, which is reported to be induced by ROS and involved in aging (1, 2, 31, 32). Indeed, the *Maf* promoter contains multiple Trp53 binding sites and overexpression of Trp53 markedly inhibited the activity of the *Maf* promoter (Supplemental Figure 24). In addition, the downregulation of *Maf* by ROS was markedly attenuated in *Trp53*$^{-/-}$ osteoblasts (Figure 6B). Although NF-κB is involved in aging (33) and activated by ROS, *Maf* expression was not restored by an NF-κB inhibitor (Supplemental Figure 25). These results suggest that the oxidative stress that accumulates with aging mediates, at least in part, the age-related decrease in *Maf* expression through Trp53.

Discussion

The molecular basis for age-related changes in higher organisms is poorly understood, particularly in the skeletal system. Although many factors have been suggested to regulate the bifurcation of osteoblasts and adipocytes, the function of a few factors has been

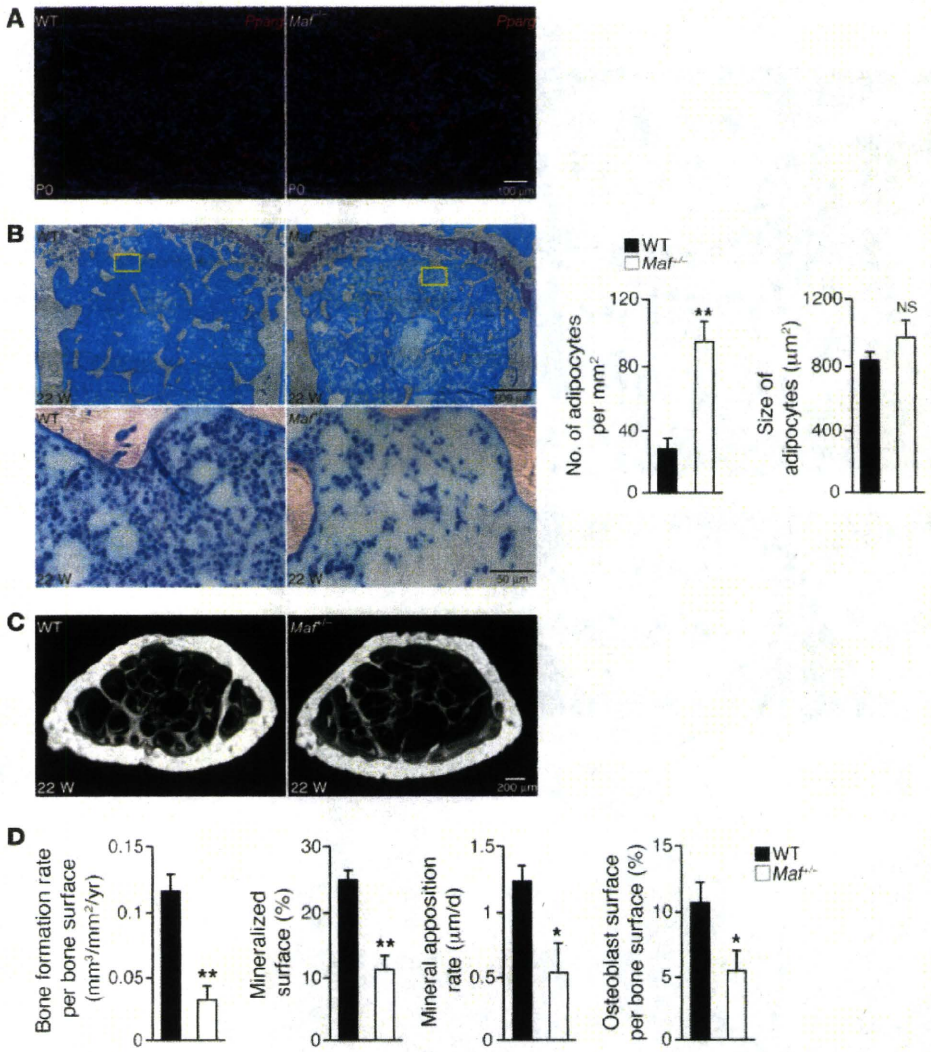

Figure 5
Increased adipogenesis in the *Maf* deficiency. (**A**) Expression of *Pparg* in the tibia of WT and *Maf*$^{-/-}$ littermates (in situ hybridization). Scale bar: 100 μm. (**B**) Histological analysis of the bone marrow of 22-week-old WT and *Maf*$^{+/-}$ female mice (femur, toluidine blue staining). Yellow boxed regions in the top panels are shown at higher magnification in the bottom panels. Note that *Maf*$^{+/-}$ bone marrow is filled with adipocytes. The number, but not the size, of adipocytes was significantly increased ($n = 6$). Scale bar: 500 μm (top row); 50 μm (bottom row). (**C**) Three-dimensional microcomputed tomography images of the femurs of 22-week-old WT and *Maf*$^{+/-}$ mice. Scale bar: 200 μm. (**D**) Parameters of osteoblastic bone formation in the bone morphometric analysis ($n = 6$; 22–26 weeks old). $^{*}P < 0.05$; $^{**}P < 0.01$.

demonstrated by genetic loss-of-function studies (7), and how the expression level of these factors changes in aging is not well known. A combination of a genome-wide screening and mouse genetic studies led us to identify the expression level of *Maf* to be both under the influence of aging and a determinant of mesenchymal cell differentiation into osteoblasts and adipocytes (Figure 6E).

Maf promotes osteoblast differentiation by regulating osteoblast genes, including *Bglap1*, in cooperation with Runx2. We propose that Maf functions as a modulator of bone formation by regulating the activity of crucial determinants like Runx2. Even in aged mice, bone marrow cells expressed a normal level of Runx2 (based on the screening shown in Figure 1A and Supplemental Table 1), but a low level of *Maf* expression resulted in a decrease in Runx2-mediated transcriptional activity. Therefore, Maf is a potential candidate to help explain the gradual and moderate decrease in bone formation observed in age-related osteoporosis. We also demonstrated that Maf inhibited adipocyte differentiation through the downregulation of *Pparg* expression, thus indicating that Maf regulates the bifurcation of the mesenchymal cell lineage into osteoblasts and adipocytes. It is interesting to note that the *MAF* locus was recently identified as one of the risk loci for obesity (34).

Using genetically modified mice, AP-1 superfamily members Fra1, Junb, and ΔFosb were shown to regulate bone formation (35–37), but ΔFosb was the only member that also regulates adipogenesis (19). However, since the adipogenic function of ΔFosb depends on a non–cell-autonomous mechanism (38), Maf is the only AP-1 superfamily member that has a cell-autonomous role in the regulation of both osteoblast and adipocyte differentiation. Interestingly, Maf also regulated osteoclastogenesis in a cell-autonomous manner, possibly by modulating NFAT activity (Sup-

Table 2
Skeletal development of 22-week-old *Maf*$^{+/-}$ mice

	WT	*Maf*$^{+/-}$
BV/TV (%)	4.43 ± 0.15	3.17 ± 0.54^{A}
Tb.N (mm^{-1})	1.90 ± 0.02	1.54 ± 0.14^{A}
Tb.Sp (μm)	503.82 ± 5.69	623.86 ± 51.19^{A}
Tb.Th (μm)	23.35 ± 0.59	20.98 ± 0.60^{A}

Microcomputed tomography analysis of the femurs of 22-week-old WT and *Maf*$^{+/-}$ mice. $^{A}P < 0.05$.

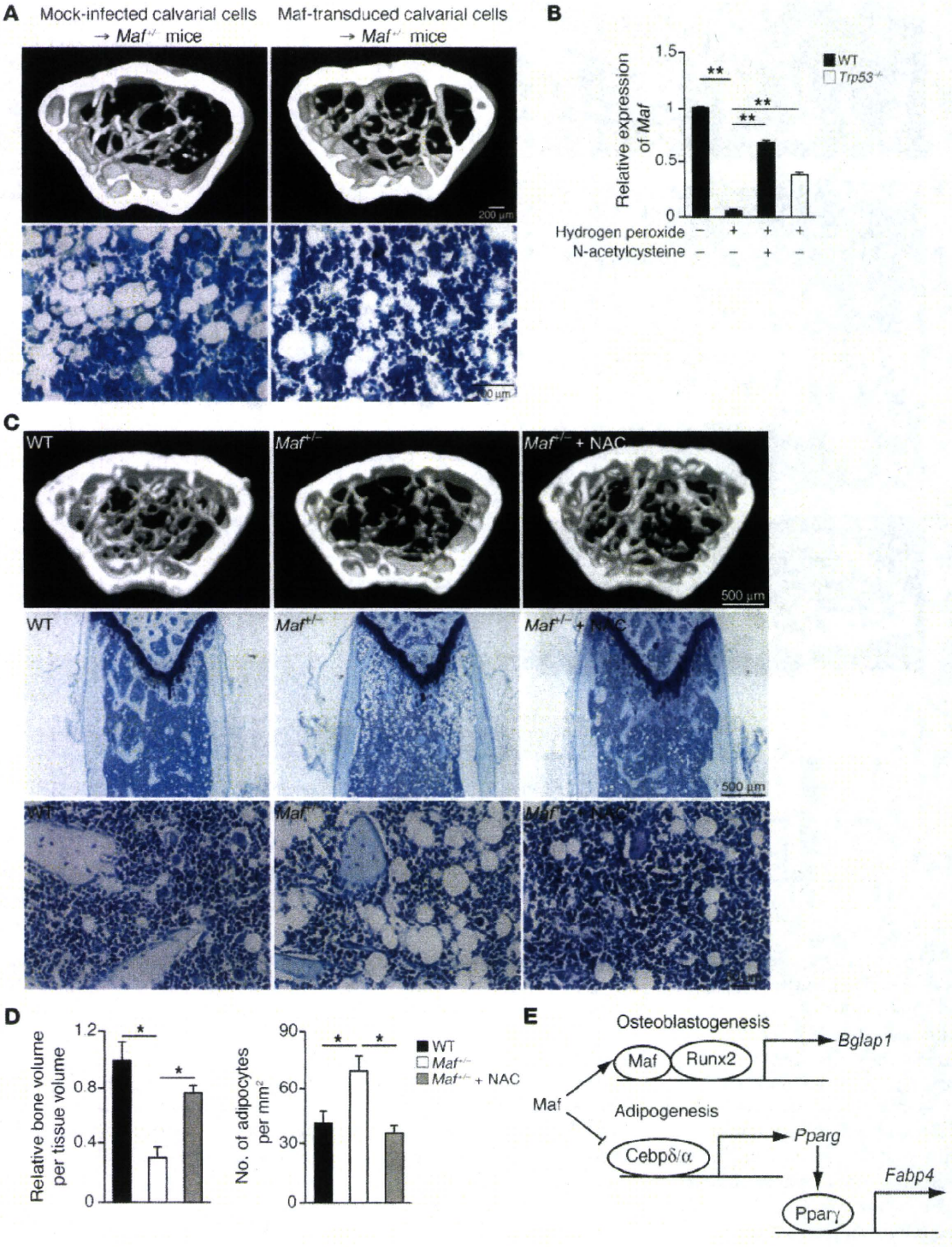

Figure 6

Aging and Maf-mediated regulation of osteoblastogenesis and adipogenesis. (**A**) Effect of Maf overexpression in mesenchymal cells on an aging phenotype of *Maf*$^{+/-}$ mice. Three-dimensional microcomputed tomography images and histological analysis of the bone marrow (toluidine blue staining) of *Maf*$^{+/-}$ mice transplanted with Maf-transduced or mock-infected calvarial cells. Scale bar: 200 μm (top row); 100 μm (bottom row). (**B**) Effect of hydrogen peroxide on *Maf* expression in WT and *Trp53*$^{-/-}$ calvarial osteoblasts (real-time RT-PCR analysis). (**C**) Effect of *N*-acetylcysteine (NAC) administration on an aging phenotype of *Maf*$^{+/-}$ mice. Three-dimensional microcomputed tomography images (top row) and histology of the bone marrow (toluidine blue staining, middle and bottom rows) of mice ($n = 4$). Images in the middle row are shown at higher magnification in the bottom row. Scale bar: 500 μm (top and middle rows); 50 μm (bottom row). (**D**) Microcomputed tomography and histological analysis of WT and *Maf*$^{+/-}$ mice. (**E**) A model of Maf-mediated reciprocal regulation of osteoblast and adipocyte differentiation. *$P < 0.05$; **$P < 0.01$.

Table 3
Skeletal development and adipogenesis in *Maf*$^{+/-}$ mice transplanted with Maf-transduced and mock-infected calvarial cells

	Mock-infected calvarial cells	Maf-transduced calvarial cells
BV/TV (%)	4.95 ± 0.77	6.81 ± 0.57[A]
CV/TV (%)	35.06 ± 0.43	35.09 ± 0.71
Adipocytes (mm^{-2})	97.1 ± 6.6	62.8 ± 6.7[B]

Effect of Maf overexpression in mesenchymal cells on an aging phenotype of *Maf*$^{+/-}$ mice (n = 4). CV/TV, cortical bone volume/total volume. [A]$P < 0.05$. [B]$P < 0.01$.

plemental Figure 5, C and E), suggesting that Maf plays a distinct role in each skeletal cell type.

Since Pparγ inhibits the expression of *Maf* (39), a small reduction in *Maf* expression would form a vicious cycle: an increasing expression of *Pparg* further inhibits *Maf* expression, leading to a severe reduction in *Maf*. Antidiabetic drugs — such as TZDs, which activate Pparγ — are known to reduce bone mass and increase fracture risk (12). Interestingly, treatment with rosiglitazone led to decreased *Maf* expression (data not shown). This is possibly because Pparγ agonists accelerate this vicious cycle through suppression of *Maf* expression.

Mathematical modeling of gene expression is helpful for understanding how the gradual reduction of *Maf* expression leads to a dramatic change in cell differentiation. Based on this simulation, if the expression of *Maf* decreased by more than 60% of the maximum level, the adipogenic genes became preferentially expressed (Supplemental Figure 26 and Supplemental Methods). Reduction of *Maf* gene expression in neonatal *Maf*$^{+/-}$ mice was not sufficient for activation of this switch, as we observed no obvious bone phenotype in neonatal *Maf*$^{+/-}$ mice (Figure 1B and Supplemental Figure 17). As the level of *Maf* gradually decreased with age, they exhibited an osteopenic phenotype with fatty marrow.

Currently, there are few drugs available in the clinic that effectively increase bone formation. The modulation of *Maf* expression appears to hold considerable promise as what we believe to be a novel antiaging therapeutic target in the skeletal system.

Methods

Mice. Maf$^{-/-}$ mice were previously generated and described elsewhere (16). *Maf*$^{-/-}$ mice were backcrossed into C57BL/6 mice for more than 9 generations, unless otherwise described. All mice were born and maintained under specific pathogen-free conditions. All animal experiments were performed with the approval of the Animal Study Committee of Tokyo Medical and Dental University and conformed to relevant guidelines and laws.

Microcomputed tomography analysis. CT scanning was performed using a ScanXmate-A100S Scanner (Comscantechno). Three-dimensional microstructural image data were reconstructed and structural indices were calculated using TRI/3D-BON software (RATOC). Bone mineral density (BMD) was calculated using TRI/3D-BON-BMD-PNTM software (RATOC). Bone morphometric and BMD analyses were performed at a region 0.8–1.8 mm above the distal growth plate of the femur in adult mice and using the full-length femur in postnatal mice, unless otherwise described.

In situ hybridization and immunohistochemical analysis. Embryos and bones were fixed in 4% paraformaldehyde, embedded in paraffin, and sectioned (5 μm). In situ hybridization was performed using ^{35}S-labeled *Bglap1*, *Runx2*, and *Col1a1* probes as described previously (40). The *Pparg* probe is a 521-bp fragment of the *Pparg* coding region. Immunohistochemical analysis was performed using a standard avidin-biotin peroxidase method (Vector Laboratories), according to the manufacturer's protocols. Paraffin-embedded sections were dewaxed, rehydrated, and subjected to an antigen retrieval procedure. The sections were then blocked with 5% lamb serum and incubated with the antibody. The antibodies are listed in Supplemental Table 2. For the proliferation assay, pregnant mice were injected with BrdU 1 hour before sacrifice. We detected mitotic cells using the BrdU Staining Kit (Zymed) and detected apoptotic cells by TUNEL staining with the ApoAlert DNA Fragmentation Kit (Clontech).

Cell cultures. For in vitro osteoblast and adipocyte differentiation, cells derived from bone marrow or calvaria were cultured with osteogenic medium (50 μM ascorbic acid, 10 nM dexamethasone, and 10 mM β-glycerophosphate) or adipogenic medium (0.5 mM 3-isobutyl-1-methylxanthine, 5 μg/ml insulin, and 1 μM dexamethasone), as described previously (20, 41). ALP assay (7 days of culture), alizarin red staining (21 days of culture), and oil red O staining (10 days of culture) were performed as previously described (20, 41). We determined the rate of cell proliferation using the Cell Proliferation ELISA kit (Roche) and detected apoptotic cells by TUNEL staining with the MEBSTATIN Apoptosis Kit Direct (MBL). The method for in vitro osteoclast differentiation was described previously (42–44). Briefly, bone marrow–, fetal liver–, or spleen-derived cells, cultured with 10 ng/ml M-CSF (R&D Systems) for 2 days, were used as osteoclast precursor cells, which were further cultured with 50 ng/ml RANKL (Peprotech) in the presence of 10 ng/ml M-CSF for 3 days. In the coculture system used to generate osteoclasts, bone marrow cells were cultured with calvarial cells in the presence of 1 nM 1,25-dihydroxyvitamin D_3 (Wako) and 1 μM prostaglandin E_2 (Cayman Chemical) for 7 days.

To obtain the stable transformants constitutively expressing Maf, the retroviral vectors pMX-HA-Maf-IRES-Puro and pMX-IRES-Puro, as the control, were introduced into C3H10T1/2 and ST2 clonal cells, and the stable transformants were selected with puromycin. To establish the stable transformants expressing shRNAs targeting Maf, the retroviral vectors pSIREN-shMaf and pSIREN-shControl were introduced into ST2 clonal cells, and stable transformants were selected with puromycin. For osteoblast and adipocyte differentiation, transformants were cultured under an osteogenic condition (50 μM ascorbic acid, 10 nM dexamethasone, 10 mM β-glycerophosphate, and 100 ng/ml BMP2) and adipogenic condition (0.26 mM 3-isobutyl-1-methylxanthine, 85 nM insulin, and 0.5 μM dexamethasone), respectively.

Transplantation of Maf-transduced calvarial cells. The transplantation experiment was performed as described previously (45) with minor modifications. Briefly, we used 32-week-old WT and *Maf*$^{+/-}$ mice as recipients and newborn *Maf*$^{-/-}$ mice as donors. The mice were obtained from an intercross between *Maf*$^{+/-}$ mice, which are backcrossed into C57BL/6 mice for more than 9 generations. The mice were anesthetized by an injection of somnopentyl into the peritoneal cavity, and the proximal femur was gently drilled with a diamond-coated burr. Cells were obtained from calvaria derived from newborn *Maf*$^{-/-}$ mice and transduced with a retroviral vector (pMX-HA-Maf-IRES-GFP or pMX-IRES-GFP). The Maf-transduced or mock-infected calvarial cells were directly injected into the bone marrow cavity through the hole in the femur using a 28-gauge needle (approximately 1×10^5 cells per femur). The needle was inserted almost to the distal metaphysis. After transplantation, the drilled hole was filled with bone cement (Fuji Lute, GC). The mice were analyzed 1 month after transplantation. Microcomputed tomography analysis and measurement of fat marrow were performed within 1 mm above the distal growth plate of the femur.

Administration of N-acetylcysteine. Maf$^{+/-}$ mice were backcrossed into C57BL/6 mice for more than 3 generations. Mice were supplied drinking water containing 2 mg/ml *N*-acetylcysteine ad libitum for 14 weeks. At 22 weeks of age, mice were sacrificed and analyzed.

RNA blot and real-time RT-PCR analyses. Total RNA was extracted with ISOGEN (Wako) or the RNeasy Lipid Tissue Mini Kit (Qiagen). Total RNA was blotted and hybridized with [α-^{32}P]dCTP-labeled probes for *Maf*, *Bglap1*, and *Gapdh*, as described previously (39, 41). Real-time RT-PCR was performed with a LightCycler (Roche) using SYBR Green (Toyobo) as described previously (44). The primer sequences are listed in Supplemental Table 3.

GeneChip analysis. GeneChip analysis, clustering analysis, and GSEA were performed as described previously (42, 46, 47). Calvarial cells cultured with osteogenic medium for 0, 7, and 21 days were analyzed. BMSCs derived from 8- and 32-week-old mice were isolated as described previously (48) with minor modifications. Briefly, bone marrow cells from each of the mice were isolated by flushing the femurs and tibiae with α-MEM with 10% FBS, and these cells were plated on plastic dishes. After 3 days, adherent cells were used. BMSCs contain a precursor of osteoblasts and adipocytes (data not shown) (49). The total RNAs extracted from these cells were used for cDNA synthesis by reverse transcription, followed by synthesis of biotinylated cRNA through in vitro transcription. After cRNA fragmentation, hybridization with the Mouse Genome 430 2.0 Array (Affymetrix) was performed as described previously (42). The main part of the data set was deposited and can be obtained from the Genome Network Platform (http://genomenetwork.nig.ac.jp/).

ChIP assay. After calvarial cells were cultured with osteogenic medium for 7 days, ChIP assay was performed using the ChIP Assay Kit (Upstate) with minor modification. The antibodies used are listed in Supplemental Table 2. The primer sequences are listed in Supplemental Table 3.

Retroviral gene transfer. Retroviral vectors pMX-HA-Maf-IRES-GFP and pMX-HA-Maf-IRES-Puro were constructed by inserting DNA fragments encoding HA and Maf into pMX-IRES-GFP and pMX-IRES-Puro (50). Retroviral vectors pSIREN-shMaf and pSIREN-shControl were constructed by inserting annealed oligonucleotide into RNAi-Ready pSIREN-RetroQ (BD Biosciences). The oligonucleotide sequences are listed in Supplemental Table 3. Retroviral packaging was performed by transfecting the plasmids into Plat-E or Plat-A cells using FuGENE6 as described previously (50).

Reporter gene assay. The reporter plasmids, *Bglap1*-luc variants, were constructed from 1050Oc-luc (41), and mutations in MARE-like sequences were introduced by PCR. A site-directed mutagenesis performed with sequential PCR steps was used to engineer the mutated MARE-like sequences. Two overlapping PCR fragments, each containing the MARE1–MARE5 mutation, were generated. The corresponding PCR fragments were used as templates for the second PCR step. The primer sequences are listed in Supplemental Table 3. *Maf*-luc was constructed by subcloning a 2-kb fragment of the 5′ flanking region of the *Maf* gene into the pGL3-basic vector (Promega). Luciferase assay was performed in NIH3T3 cells or mouse embryonic fibroblasts (MEFs) established from WT and *Runx2*$^{-/-}$ E14 embryos (51). *Pparg*-luc was constructed by subcloning a 2.2-kb fragment of the 5′ flanking region of the *Pparg* gene (52) into the pGL3-basic vector, and mutations in MAREs were introduced by PCR. The primer sequences are listed in Supplemental Table 3. Luciferase assay was performed in 3T3-L1 cells. The expression plasmids of Maf, Runx2, Fos, Fosb, Fosl1, Fosl2, Jun, Junb, Jund, Cebpα, Cebpβ, Cebpδ, Crebbp, p50, p65, and Tp53 have been described elsewhere (16, 41, 42, 53–58). The expression plasmids of ΔFosb and Δ2ΔFosb were constructed from full-length Fosb cDNA using PCR. The reporter plasmids (p*Acp5*-luc, ref. 42, and p*Nfatc1*-luc, ref. 43) were described previously. MEFs and NIH3T3 and 3T3-L1 cells were transfected using Lipofectamine plus reagents (Invitrogen). After 30–36 hours, dual luciferase assay was performed according to the manufacturer's protocols (Promega).

Immunoblot and immunoprecipitation analyses. Immunoblot and immunoprecipitation analyses were performed as previously described (59). The antibodies used are listed in Supplemental Table 2. For analyzing the interaction between Maf and Runx2, HA-tagged Maf, HA-tagged N-terminal region of Maf (HA-tagged MafΔC), HA-tagged C-terminal region of Maf (HA-tagged MafΔN), HA-tagged Runx2, HA-tagged Runx2ΔN, HA-tagged Runx2ΔC, FLAG-tagged Maf, and FLAG-tagged Runx2 proteins were produced by the in vitro transcription/translation system (Promega). These proteins were mixed in a binding buffer and incubated with anti-FLAG antibody-conjugated agarose beads (Sigma-Aldrich). Recovered proteins were subjected to immunoblot analysis with anti-FLAG and anti-HA antibodies. For analyzing the interaction among Maf, Cebpδ, and Crebbp, HA-tagged Maf and Cebpδ proteins were produced by the in vitro transcription/translation system. FLAG-tagged Crebbp proteins were produced by transfecting FLAG-Crebbp expression plasmids into HEK293T cells using FuGENE6 (Roche). These proteins were mixed and incubated with anti-FLAG antibody-conjugated agarose beads. Recovered proteins were subjected to immunoblot analysis with anti-Cebpδ, anti-FLAG, and anti-HA antibodies.

Treatment of Trp53$^{-/-}$ *osteoblasts with hydrogen peroxide.* Osteoblasts were isolated from the calvaria of newborn mice deficient in *Trp53* (accession no., CDB0001K; http://www.cdb.riken.jp/arg/mutant%20mice%20list.html) (60) and treated with 600 μM hydrogen peroxide. Five days after the treatment, mRNAs were extracted and subjected to real-time PCR analysis.

EMSA. EMSA was performed as previously described (59). Maf and Cebpδ proteins were produced by the in vitro transcription/translation system. The CCAAT probe for binding of Cebpδ and the MARE probe for binding of Maf were generated by annealing synthetic oligonucleotides. The oligonucleotide sequences are listed in Supplemental Table 3. Antibodies against Maf and Cebpδ were used for supershift analysis.

ELISA. Soluble osteocalcin levels and TRAP activity in serum were detected using the mouse osteocalcin EIA kit (Biomedical Technologies Inc.) and mouse TRAP assay (SBA Sciences), respectively.

Statistics. Statistical analysis was performed using Student's *t* test for comparisons between 2 groups and analysis of variance with Bonferroni post-hoc test for comparisons among 3 or more groups, unless otherwise described. All data are expressed as mean ± SEM.

Acknowledgments

We thank H.R. Ueda, M. Asagiri, T. Ando, Y. Kunisawa, T. Honda, Y. Suzuki, T. Kudo, A. Izumi, A. Suematsu, and A. Hirota for discussion and assistance. This work was supported in part by a grant for ERATO from the Takayanagi Osteonetwork Project from the Japan Science and Technology Agency; Grant-in-Aids for Creative Scientific Research and Young Scientist (A and Start-up) from the Japan Society for the Promotion of Science (JSPS); Grant-in-Aid for Challenging Exploratory Research JSPS; grants for the Genome Network Project and Global Center of Excellence Program from the Ministry of Education, Culture, Sports, Science and Technology of Japan; and grants from Tokyo Biochemical Research Foundation, Life Science Foundation of Japan, Yokoyama Foundation for Clinical Pharmacology, and Takeda Science Foundation.

Received for publication February 1, 2010, and accepted in revised form July 14, 2010.

Address correspondence to: Hiroshi Takayanagi, Department of Cell Signaling, Graduate School of Medical and Dental Sciences, Tokyo Medical and Dental University, Yushima 1-5-45, Bunkyo-ku, Tokyo 113-8549, Japan. Phone: 81.3.5803.5471; Fax: 81.3.5803.0192; E-mail: taka.csi@tmd.ac.jp.

1. Collado M, Blasco MA, Serrano M. Cellular senescence in cancer and aging. *Cell.* 2007;130(2):223–233.
2. Chen JH, Hales CN, Ozanne SE. DNA damage, cellular senescence and organismal ageing: causal or correlative? *Nucleic Acids Res.* 2007;35(22):7417–7428.
3. Uccelli A, Moretta L, Pistoia V. Mesenchymal stem cells in health and disease. *Nat Rev Immunol.* 2008;8(9):726–736.
4. Engler AJ, Sen S, Sweeney HL, Discher DE. Matrix elasticity directs stem cell lineage specification. *Cell.* 2006;126(4):677–689.
5. Meunier P, Aaron J, Edouard C, Vignon G. Osteoporosis and the replacement of cell populations of the marrow by adipose tissue. A quantitative study of 84 iliac bone biopsies. *Clin Orthop Relat Res.* 1971; 80:147–154.
6. Manolagas SC. Birth and death of bone cells: basic regulatory mechanisms and implications for the pathogenesis and treatment of osteoporosis. *Endocr Rev.* 2000;21(2):115–137.
7. Gimble JM, Zvonic S, Floyd ZE, Kassem M, Nuttall ME. Playing with bone and fat. *J Cell Biochem.* 2006;98(2):251–266.
8. Belaid-Choucair Z, et al. Human bone marrow adipocytes block granulopoiesis through neuropilin-1-induced granulocyte colony-stimulating factor inhibition. *Stem Cells.* 2008;26(6):1556–1564.
9. Corre J, Planat-Benard V, Corberand JX, Penicaud L, Casteilla L, Laharrague P. Human bone marrow adipocytes support complete myeloid and lymphoid differentiation from human CD34 cells. *Br J Haematol.* 2004;127(3):344–347.
10. Maurin AC, Chavassieux PM, Frappart L, Delmas PD, Serre CM, Meunier PJ. Influence of mature adipocytes on osteoblast proliferation in human primary cocultures. *Bone.* 2000;26(5):485–489.
11. Naveiras O, Nardi V, Wenzel PL, Hauschka PV, Fahey F, Daley GQ. Bone-marrow adipocytes as negative regulators of the haematopoietic microenvironment. *Nature.* 2009;460(7252):259–263.
12. McDonough AK, Rosenthal RS, Cao X, Saag KG. The effect of thiazolidinediones on BMD and osteoporosis. *Nat Clin Pract Endocrinol Metab.* 2008; 4(9):507–513.
13. Seeman E, Delmas PD. Bone quality--the material and structural basis of bone strength and fragility. *N Engl J Med.* 2006;354(21):2250–2261.
14. Lamberts SW, van den Beld AW, van der Lely AJ. The endocrinology of aging. *Science.* 1997; 278(5337):419–424.
15. Rosen CJ. Growth hormone, insulin-like growth factors, and the senescent skeleton: Ponce de Leon's Fountain revisited? *J Cell Biochem.* 1994; 56(3):348–356.
16. Kawauchi S, et al. Regulation of lens fiber cell differentiation by transcription factor c-Maf. *J Biol Chem.* 1999;274(27):19254–19260.
17. Ho IC, Glimcher LH. Transcription: tantalizing times for T cells. *Cell.* 2002;109 suppl:S109–S120.
18. MacLean HE, Kim JI, Glimcher MJ, Wang J, Kronenberg HM, Glimcher LH. Absence of transcription factor c-maf causes abnormal terminal differentiation of hypertrophic chondrocytes during endochondral bone development. *Dev Biol.* 2003;262(1):51–63.
19. Sabatakos G, et al. Overexpression of DeltaFosB transcription factor(s) increases bone formation and inhibits adipogenesis. *Nat Med.* 2000;6(9):985–990.
20. Hong JH, et al. TAZ, a transcriptional modulator of mesenchymal stem cell differentiation. *Science.* 2005;309(5737):1074–1078.
21. Karsenty G, Wagner EF. Reaching a genetic and molecular understanding of skeletal development. *Dev Cell.* 2002;2(4):389–406.
22. Yang X, et al. ATF4 is a substrate of RSK2 and an essential regulator of osteoblast biology; implication for Coffin-Lowry Syndrome. *Cell.* 2004; 117(3):387–398.
23. Montecino M, Lian J, Stein G, Stein J. Changes in chromatin structure support constitutive and developmentally regulated transcription of the bone-specific osteocalcin gene in osteoblastic cells. *Biochemistry.* 1996;35(15):5093–5102.
24. Lee CH, Olson P, Evans RM. Minireview: lipid metabolism, metabolic diseases, and peroxisome proliferator-activated receptors. *Endocrinology.* 2003; 144(6):2201–2207.
25. Farmer SR. Transcriptional control of adipocyte formation. *Cell Metab.* 2006;4(4):263–273.
26. Tontonoz P, Spiegelman BM. Fat and beyond: the diverse biology of PPARgamma. *Annu Rev Biochem.* 2008;77:289–312.
27. Shi XM, Blair HC, Yang X, McDonald JM, Cao X. Tandem repeat of C/EBP binding sites mediates PPARgamma2 gene transcription in glucocorticoid-induced adipocyte differentiation. *J Cell Biochem.* 2000;76(3):518–527.
28. Wu Z, et al. Cross-regulation of C/EBP alpha and PPAR gamma controls the transcriptional pathway of adipogenesis and insulin sensitivity. *Mol Cell.* 1999;3(2):151–158.
29. Kovacs KA, Steinmann M, Magistretti PJ, Halfon O, Cardinaux JR. CCAAT/enhancer-binding protein family members recruit the coactivator CREB-binding protein and trigger its phosphorylation. *J Biol Chem.* 2003;278(38):36959–36965.
30. Nakanishi R, et al. Secreted frizzled-related protein 4 is a negative regulator of peak BMD in SAMP6 mice. *J Bone Miner Res.* 2006;21(11):1713–1721.
31. Almeida M, et al. Skeletal involution by age-associated oxidative stress and its acceleration by loss of sex steroids. *J Biol Chem.* 2007;282(37):27285–27297.
32. Tyner SD, et al. p53 mutant mice that display early ageing-associated phenotypes. *Nature.* 2002; 415(6867):45–53.
33. Adler AS, Sinha S, Kawahara TL, Zhang JY, Segal E, Chang HY. Motif module map reveals enforcement of aging by continual NF-kappaB activity. *Genes Dev.* 2007;21(24):3244–3257.
34. Meyre D, et al. Genome-wide association study for early-onset and morbid adult obesity identifies three new risk loci in European populations. *Nat Genet.* 2009;41(2):157–159.
35. Jochum W, et al. Increased bone formation and osteosclerosis in mice overexpressing the transcription factor Fra-1. *Nat Med.* 2000;6(9):980–984.
36. Eferl R, et al. The Fos-related antigen Fra-1 is an activator of bone matrix formation. *EMBO J.* 2004; 23(14):2789–2799.
37. Kenner L, et al. Mice lacking JunB are osteopenic due to cell-autonomous osteoblast and osteoclast defects. *J Cell Biol.* 2004;164(4):613–623.
38. Rowe GC, Choi CS, Neff L, Horne WC, Shulman GI, Baron R. Increased energy expenditure and insulin sensitivity in the high bone mass DeltaFosB transgenic mice. *Endocrinology.* 2009;150(1):135–143.
39. Serria MS, Ikeda H, Omoteyama K, Hirokawa J, Nishi S, Sakai M. Regulation and differential expression of the c-maf gene in differentiating cultured cells. *Biochem Biophys Res Commun.* 2003; 310(2):318–326.
40. Takeda S, Bonnamy JP, Owen MJ, Ducy P, Karsenty G. Continuous expression of Cbfa1 in nonhypertrophic chondrocytes uncovers its ability to induce hypertrophic chondrocyte differentiation and partially rescues Cbfa1-deficient mice. *Genes Dev.* 2001; 15(4):467–481.
41. Kim S, et al. Stat1 functions as a cytoplasmic attenuator of Runx2 in the transcriptional program of osteoblast differentiation. *Genes Dev.* 2003; 17(16):1979–1991.
42. Takayanagi H, et al. Induction and activation of the transcription factor NFATc1 (NFAT2) integrate RANKL signaling in terminal differentiation of osteoclasts. *Dev Cell.* 2002;3(6):889–901.
43. Asagiri M, et al. Autoamplification of NFATc1 expression determines its essential role in bone homeostasis. *J Exp Med.* 2005;202(9):1261–1269.
44. Nishikawa K, et al. Blimp1-mediated repression of negative regulators is required for osteoclast differentiation. *Proc Natl Acad Sci U S A.* 2010; 107(7):3117–3122.
45. Zhang XS, et al. Local ex vivo gene therapy with bone marrow stromal cells expressing human BMP4 promotes endosteal bone formation in mice. *J Gene Med.* 2004;6(1):4–15.
46. Eisen MB, Spellman PT, Brown PO, Botstein D. Cluster analysis and display of genome-wide expression patterns. *Proc Natl Acad Sci U S A.* 1998; 95(25):14863–14868.
47. Subramanian A, et al. Gene set enrichment analysis: a knowledge-based approach for interpreting genome-wide expression profiles. *Proc Natl Acad Sci U S A.* 2005;102(43):15545–15550.
48. Xiao Y, Fu H, Prasadam I, Yang YC, Hollinger JO. Gene expression profiling of bone marrow stromal cells from juvenile, adult, aged and osteoporotic rats: with an emphasis on osteoporosis. *Bone.* 2007;40(3):700–715.
49. Holmes C, Khan TS, Owen C, Ciliberti N, Grynpas MD, Stanford WL. Longitudinal analysis of mesenchymal progenitors and bone quality in the stem cell antigen-1-null osteoporotic mouse. *J Bone Miner Res.* 2007;22(9):1373–1386.
50. Morita S, Kojima T, Kitamura T. Plat-E: an efficient and stable system for transient packaging of retroviruses. *Gene Ther.* 2000;7(12):1063–1066.
51. Otto F, et al. Cbfa1, a candidate gene for cleidocranial dysplasia syndrome, is essential for osteoblast differentiation and bone development. *Cell.* 1997;89(5):765–771.
52. Kudo M, Sugawara A, Uruno A, Takeuchi K, Ito S. Transcription suppression of peroxisome proliferator-activated receptor gamma2 gene expression by tumor necrosis factor alpha via an inhibition of CCAAT/ enhancer-binding protein delta during the early stage of adipocyte differentiation. *Endocrinology.* 2004;145(11):4948–4956.
53. Nishiyori A, et al. Determination of tissue specificity of the enhancer by combinatorial operation of tissue-enriched transcription factors. Both HNF-4 and C/EBP beta are required for liver-specific activity of the ornithine transcarbamylase enhancer. *J Biol Chem.* 1994;269(2):1323–1331.
54. Matsuo K, Owens JM, Tonko M, Elliott C, Chambers TJ, Wagner EF. Fosl1 is a transcriptional target of c-Fos during osteoclast differentiation. *Nat Genet.* 2000;24(2):184–187.
55. Ohoka N, Yoshii S, Hattori T, Onozaki K, Hayashi H. TRB3, a novel ER stress-inducible gene, is induced via ATF4-CHOP pathway and is involved in cell death. *EMBO J.* 2005;24(6):1243–1255.
56. Kawai J, et al. Functional annotation of a full-length mouse cDNA collection. *Nature.* 2001; 409(6821):685–690.
57. Koga T, et al. NFAT and Osterix cooperatively regulate bone formation. *Nat Med.* 2005;11(8):880–885.
58. Tanikawa J, et al. p53 suppresses the c-Myb-induced activation of heat shock transcription factor 3. *J Biol Chem.* 2000;275(20):15578–15585.
59. Nishikawa K, et al. Self-association of Gata1 enhances transcriptional activity in vivo in zebra fish embryos. *Mol Cell Biol.* 2003;23(22):8295–8305.
60. Tsukada T, et al. Enhanced proliferative potential in culture of cells from p53-deficient mice. *Oncogene.* 1993;8(12):3313–3322.

THE JOURNAL OF BIOLOGICAL CHEMISTRY VOL. 285, NO. 37, pp. 28826–28837, September 10, 2010

Deficiency of Chemokine Receptor CCR1 Causes Osteopenia Due to Impaired Functions of Osteoclasts and Osteoblasts*[S]

Received for publication, December 30, 2009, and in revised form, May 27, 2010 Published, JBC Papers in Press, June 22, 2010, DOI 10.1074/jbc.M109.099424

Akiyoshi Hoshino,[a,b,c1] Tadahiro Iimura,[d2,3] Satoshi Ueha,[e] Sanshiro Hanada,[a] Yutaka Maruoka,[a,f4] Mitsuori Mayahara,[g] Keiko Suzuki,[h] Toshio Imai,[i] Masako Ito,[j] Yoshinobu Manome,[c] Masato Yasuhara,[b] Takaaki Kirino,[k] Akira Yamaguchi,[d2] Kouji Matsushima,[e5] and Kenji Yamamoto[a,b6]

From the [a]International Clinical Research Center, Research Institute, International Medical Center of Japan, Tokyo 162-8655, the [e]Department of Molecular Preventive Medicine, Graduate School of Medicine, The University of Tokyo, Tokyo 113-0033, the Departments of [b]Pharmacokinetics and Pharmacodynamics (Hospital Pharmacy) and [d]Oral Pathology, Global Center of Excellence, Tokyo Medical and Dental University, Tokyo 113-8519, the [c]Department of Molecular Cell Biology, Institute of DNA Medicine, Research Center for Medical Sciences, Jikei University School of Medicine, Tokyo 105-8461, the [f]Department of Dentistry and Oral Surgery, Toyama National Hospital, International Medical Center of Japan, Tokyo 162-8655, the Departments of [g]Oral Histology and [h]Pharmacology, Showa University School of Dentistry, Tokyo 142-8555, the [i]Kan Research Institute, Inc., Kobe 650-0047, the [j]Department of Radiology, Nagasaki University School of Medicine, Nagasaki 852-8501, and the [k]International Medical Center of Japan, Tokyo 162-8655, Japan

Chemokines are characterized by the homing activity of leukocytes to targeted inflammation sites. Recent research indicates that chemokines play more divergent roles in various phases of pathogenesis as well as immune reactions. The chemokine receptor, CCR1, and its ligands are thought to be involved in inflammatory bone destruction, but their physiological roles in the bone metabolism *in vivo* have not yet been elucidated. In the present study, we investigated the roles of CCR1 in bone metabolism using CCR1-deficient mice. *Ccr1*$^{-/-}$ mice have fewer and thinner trabecular bones and low mineral bone density in cancellous bones. The lack of CCR1 affects the differentiation and function of osteoblasts. *Runx2*, *Atf4*, *Osteopontin*, and *Osteonectin* were significantly up-regulated in *Ccr1*$^{-/-}$ mice despite sustained expression of *Osterix* and reduced expression of *Osteocalcin*, suggesting a lower potential for differentiation into mature osteoblasts. In addition, mineralized nodule formation was markedly disrupted in cultured osteoblastic cells isolated from *Ccr1*$^{-/-}$ mice. Osteoclastogenesis induced from cultured *Ccr1*$^{-/-}$ bone marrow cells yielded fewer and smaller osteoclasts due to the abrogated cell-fusion. *Ccr1*$^{-/-}$ osteoclasts exerted no osteolytic activity concomitant with reduced expressions of *Rank* and its downstream targets, implying that the defective osteoclastogenesis is involved in the bone phenotype in *Ccr1*$^{-/-}$ mice. The co-culture of wild-type osteoclast precursors with *Ccr1*$^{-/-}$ osteoblasts failed to facilitate osteoclastogenesis. This finding is most likely due to a reduction in *Rankl* expression. These observations suggest that the axis of CCR1 and its ligands are likely to be involved in cross-talk between osteoclasts and osteoblasts by modulating the RANK-RANKL-mediated interaction.

Chemokines are initially identified as small cytokines that direct the homing of circulating leukocytes into sites of inflammation (1). Chemokines are now recognized to be major factors in inflammation and immune development as well as tumor growth, angiogenesis, and osteolysis. Chemokine receptors are expressed in a well organized spatiotemporal manner in various types of leukocytes, including lymphocytes, granulocytes, and macrophages. They facilitate the recruitment of these cells into inflammatory sites during the appropriate phase of inflammation.

Recent findings indicate that chemokine receptors, including CCR1[7] and its related chemokines, CCL3 and CCL9, are involved in the pathogenesis of a variety of diseases. In particular, CCL3 (also called MIP-1α), a major pro-inflammatory chemokine produced at inflammatory sites, appears to play a crucial role in pathological osteoclastogenesis (2, 3). In osteolytic bone inflammation (*e.g.* rheumatoid arthritis-associated bone destruction), CCL3 induces ectopic osteoclastogenesis (4)

* This work was supported in part by Grant H19-nano-012 from the Ministry of Health, Labor and Welfare (to K. Y.) and by a research fellowship from the Japan Society for the Promotion of Science for Young Scientists (2007–2009) (to A. H.).

[S] The on-line version of this article (available at http://www.jbc.org) contains supplemental Figs. 1–3.

[1] Supported by grants from the Japan Foundation of Cardiovascular Research (2006) and from the Naito Foundation (2005).

[2] Supported by a grant from the Japanese Ministry of Education, Global Center of Excellence Program, International Research Center for Molecular Science in Tooth and Bone Diseases.

[3] Supported by The Takeda Science Foundation, The Mochida Memorial Foundation for Medical and Pharmaceutical Research, and a Grant-in-Aid for Scientific Research from the Japan Society for the Promotion of Science (21659426).

[4] Supported by Grants H21-nanchi-097 and H22-nanchi-ippan157 from the Ministry of Health, Labor and Welfare.

[5] Supported by Solution Oriented Research for Science and Technology and by Japan Science and Technology Corp.

[6] To whom correspondence should be addressed: International Clinical Research Center, Research Institute, International Medical Center of Japan, Toyama 1-21-1, Shinjuku-ku, Tokyo 162-8655, Japan. Tel.: 81-3-3202-7181 (ext: 2856 or 5611); E-mail: backen@ri.ncgm.go.jp.

[7] The abbreviations used are: CCR, C-C chemokine receptor; M-CSF, macrophage-colony stimulation factor; BALP, bone-specific alkaline phosphatase; CCL, C-C chemokine ligand; MCP-1, macrophage chemoattractant protein-1; MIP-1, macrophage inflammatory protein-1; CT, computed tomography; PTX, pertussis toxin from *Bordetella pertussis*; RANK, receptor activator of NF-κB; RANKL, receptor activator of NF-κB ligand; RANTES, regulated upon activation normal T expression and secreted; TRAP, tartrate-resistant acid phosphatase; NTx, N-telopeptides.

and results in bone destruction (5). Several reports suggested that CCL3 is also produced by myeloma cells and directly stimulates bone destruction in myeloma-related bone diseases (5–7). These findings indicate the possible roles of CCL3 as a crucial chemokine for osteoclast function. Several antagonists of the chemokine ligands of CCL3, such as CCR1-specific (BX471) and CCR5-specific (TAK779) blockers, have been tested as drug candidates for the treatment of patients with rheumatoid arthritis-associated bone destruction and multiple myeloma (4, 8). The chemokine CCL9 (also called MIP-1γ), is also abundantly produced by various myeloid lineage-derived cells, including osteoclasts (9), activates osteoclastogenesis through its receptor, CCR1 (10–12). However, the exact physiological functions of CCR1 and its related chemokines in bone remodeling are still not fully characterized (12, 13).

A recent study using an ovariectomy-induced bone loss model found that the chemokine receptor CCR2 was associated with postmenopausal bone loss (14), but there are few reports on bone phenotypes in other chemokine receptor-deficient mouse models. In the present study, we demonstrated that osteopenia in *Ccr1*$^{-/-}$ mice appeared to be due to impaired osteoclast and osteoblast function. Our data also uncovered a possible role for CCR1 and its related ligands in the communication between osteoclasts and osteoblasts.

EXPERIMENTAL PROCEDURES

Mice—Standard male C57BL/6 mice (6–9 weeks of age) were obtained from CLEA Japan. *Ccr1*$^{-/-}$ mice (15) purchased from Jackson Laboratories were backcrossed for 8–10 generations on the C57BL/6 background mice. Mice were all bred and maintained under pathogen-free conditions at the animal facilities of the University of Tokyo. All experiments were performed according to the Institutional Guidelines for the Care and Use of Laboratory Animals in Research and were approved by the ethics committees of both the University of Tokyo and the Research Institute of International Medical Center of Japan.

Materials—Recombinant mouse M-CSF and RANKL were purchased from R&D Systems Inc. (Minneapolis, MN) and PeproTech Inc. (Rocky Hill, NJ), respectively. Recombinant mouse CCL2 (MCP-1), CCL3 (MIP-1α), CCL4 (MIP-1β), CCL5 (RANTES), CCL9 (MIP-1γ), and CCL11 (eotaxin-1) and their corresponding-neutralizing antibodies were purchased from R&D Systems. Control rat IgG was purchased from Jackson ImmunoResearch (Bar Harbor, ME). Recombinant mouse CX3CL1 (fractalkine) was purchased from R&D Systems. Hamster anti-CX3CL1-neutralizing antibody and control hamster IgG were kindly provided by Dr. Toshio Imai (Kan Research Institute, Kobe, Japan). Rabbit anti-human/mouse CCR1 polyclonal antibody and control rabbit IgG were purchased from AbCam (Cambridge, MA) and Chemicon (Temecula, CA), respectively. Secondary antibodies (Alexa488-labeled anti-rabbit IgG and Streptavidin-PE) were purchased from Molecular Probes (Eugene, OR). Rabbit anti-TRAP and anti-Cathepsin K polyclonal antibodies were both purchased from Santa Cruz Biotechnology (Santa Cruz, CA).

Osteoclast and Osteoblastic Cell Culture—Mouse bone marrow cells cultured in α-minimal essential medium were used as sources of osteoclastic and osteoblastic cell cultures. The non-adherent cells were collected for bone marrow-derived macrophage and pre-osteoclast induction, and adherent bone marrow-derived mesenchymal stromal cells were collected for osteoblast induction. Bone marrow-derived macrophages were induced with 10 ng/ml M-CSF for an additional 10 days. To generate pre-osteoclasts, non-adherent cells were passed through a column filled with Sephadex G-10 microspheres (Amersham Biosciences) and were then cultured with 10 ng/ml M-CSF and 20 ng/ml RANKL for 4 days. The mature osteoclasts were induced from pre-osteoclasts by culturing for an additional 14 days with M-CSF and RANKL. The culture media were replaced every 3 days. TRAP activity in the osteoclasts was determined by staining using an acid phosphatase leukocyte staining kit (Sigma). The contamination of stromal/osteoblastic cells was monitored using Q-PCR analysis, as a low expression level of the *Osteoprotegrin* gene indicates stromal/osteoblastic cells.

Osteoblastic differentiation in adherent bone marrow mesenchymal stromal cells was induced by culture in α-minimal essential medium containing 10% FBS, 200 μM ascorbic acid, 10 mM β-glycerophosphate, and 10 nM dexamethasone (16). The culture media was replaced once every 3 days in the presence or absence of chemokine-neutralizing antibodies. The cells were fixed with 4% paraformaldehyde and stained for alkaline phosphatase with naphthol AS-MX phosphate plus Fastblue-BB (Sigma) and for minerals with alizarin red. Mineral deposition was alternatively identified by von Kossa staining (Polysciences, Inc., Warrington, PA), and the mineralized areas were measured by using an Array Scan VTI HCS analyzer (Beckman Coulter).

Co-culture experiments with osteoclast precursors and osteoblasts were performed by inoculating bone marrow-derived precursors (1×10^5 cells/well) onto the layer of osteoblastic cells that had been cultured for 21 days with osteoblast-inducing media in 24-well plates. Thereafter, these cells were co-cultured for 7 days in α-minimal essential medium supplemented with 10% FBS and 10 μg/ml vitamin D_3. To assess bone resorption activity, these co-culture studies were also conducted using bone slices. After fixation of the cells with 2.5% glutaraldehyde/1.6% paraformaldehyde in 0.1 M cacodylic acid (pH 7.4), the bone slices were briefly rinsed, and were completely dehydrated in an ascending series of ethanol and liquid carbon dioxide. The samples were coated with an ultrafine titanium oxide powder and observed under a scanning electron microscopy.

Immunohistochemical Staining—For the immunohistochemical staining analyses, osteoclasts were fixed with 4% paraformaldehyde, permeabilized, and stained with the indicated specific antibodies, followed by Alexa594-conjugated secondary antibodies and Alexa488-labeled phalloidin (Molecular Probes). The osteoclasts with multiple nuclei (>3) were quantified. Images were captured using an IX-81 fluorescence microscope equipped with a confocal microscopy DSU unit (Olympus, Japan) and were analyzed with the MetaMorph™ software program (Universal Imaging, Molecular Devices, Sunnyvale, CA). The formation of osteoclasts was quantified by capturing and analyzing images using the ImageJ software program (National Institutes of Health, Bethesda, MD) based on

TRAP staining of 25 fields in each well, which were randomly chosen and analyzed.

Real-time PCR Analysis—Total cellular RNA from osteoclasts, osteoblasts, and bone tissues (proximal tibia after the bone marrow flush and the removal of metaphysial regions) was isolated using the RNeasy kit (Qiagen, Valencia, CA). The total RNA was then reverse-transcribed into cDNA using the Superscript III RT kit (Invitrogen). The real-time quantitative PCR analyses were performed using the ABI 7700 sequence detector system with SYBR Green (Applied Biosystems, Foster City, CA). The sequences were amplified for 40 cycles under the following conditions: denaturation at 95 °C for 15 s, annealing at 60 °C for 30 s, and extension at 72 °C for 45 s with primers for the chemokine receptors as previously reported (17). Gene expression levels were compared with *Gapdh* gene expression by the $2^{-\Delta(C_t)}$ method.

Measurement of Cytokines and Chemokines—Chemokine CCL5 and CCL9 secretion levels were determined by ELISA using the antibodies MAB4781 and BAF478 (R&D systems) and MAB463 and BAF463 (R&D systems), respectively. The reaction intensities were determined by using HRP-conjugated streptavidin (Chemicon). The cytokine production levels were quantified with a mouse 23-plex multiple cytokine detection system (Bio-Rad Corp., Hercules, CA) according to the manufacturer's instructions.

Flow Cytometry—FITC-, PE-, APC-, PerCP-Cy5.5-, PE-Cy7-, or biotin-conjugated anti-mouse mAbs to CD45.2 (104), CD115 (AFS98), and CD265/RANK (R12–31), and subclass-matched control antibodies were purchased from eBioscience (San Diego, CA). Anti-mouse mAbs to FcγR (2.4G2), Ly6C/6G (RB6–8C5), CD11b (M1/70), and CD19 (1D3) were purchased from BD Pharmingen (San Diego, CA). The flow cytometric analyses were performed using an LSR II flow cytometer with the FACS diva software program (BD Biosciences) and were analyzed with the FlowJo software program (TreeStar, Ashland, OR). Dead cells were excluded on the basis of the forward and side scatter profiles and propidium iodide staining.

Microcomputed Tomography and Peripheral Quantitative Computed Tomography—Micro-computed tomography (microCT) scanning was performed on proximal tibiae by μCT-40 (SCANCO Medical AG) with a resolution of 12 μm, and the microstructure parameters were three-dimensionally calculated as previously described (18). The bone scores were measured by peripheral quantitative CT using the XCT Research SA+ system (Stratec Medizintechnik GmbH, Pforzheim, Germany). The bone scores and density were measured and analyzed at 1.2 mm below the epiphyseal plate of distal femora. The scores were defined according to the American Society for Bone and Mineral Research standards.

Bone Histomorphometry—The unilateral proximal tibiae fixed with ethanol were embedded in glycol methacrylate, and the blocks were cut in 5-μm-thick sections. The structural parameters were analyzed at the secondary spongiosa. For the assessment of dynamic histomorphometric indices, calcein (at a dose of 20 mg/kg body weight) was injected twice (72-h interval) to wild-type and *Ccr1*-deficient mice, respectively. The sections were stained with toluidine blue and analyzed using a semi-automated system (Osteoplan II, Zeiss). The nomenclature, symbols, and units used in the present study are those recommended by the Nomenclature Committee of the American Society for Bone and Mineral Research (19).

Measurement of TRAP, BALP, and Collagen-type I N-telopeptides (NTx)—Tartrate-resistant acid phosphatases (TRAP5b) in serum and culture supernatant were measured by the mouse TRAP EIA assay kit (Immunodiagnostic system, Fountain Hills, AZ). In brief, the culture supernatant or diluted serum was applied to an anti-TRAP5b-coated microplate, according to the manufacturer's instruction. The enzymatic activities of bound TRAP were determined with chromogenic substrates. Bone-specific alkaline phosphatase (BALP) levels were measured using the mouse BALP ELISA kit (Cusabio Biotech Co. Ltd., Wilmington, DE). Collagen-type I NTx were measured by ELISA (SRL, Tokyo).

Collagen-based Zymography—Collagen digestion activity was measured by using modified methods, which were based on gelatin-based zymography (20), with some modification for type-I collagen (21, 22). In brief, the osteoclasts were gently digested with lysis buffer (150 mM NaCl, 50 mM HEPES, 5 mM EDTA, and 10% Nonidet P-40 with Halt protease inhibitor mixture, pH 7.5). The lysates were separated by SDS-PAGE on a 10% polyacrylamide gel with porcine type-I collagen (1 mg/ml, Nitta Gelatin Inc., Osaka, Japan) under chilled conditions. The gel was washed with denaturation buffer (Tris-buffered saline (150 mM NaCl, 25 mM Tris-HCl, pH 7.4, supplemented with 2.5% Triton X-100) and then subjected to zymography for 18–24 h at 37 °C in zymography developing buffer (Tris-buffered saline, supplemented with 1 mM $CaCl_2$, 1 μM $ZnCl_2$, and 0.05% Brij-35). The signals were detected using Coomassie Brilliant Blue solution (Wako Pure Chemicals, Osaka, Japan).

Immunoblot Analysis—Total cell lysates were isolated, separated by SDS-PAGE, and electrotransferred onto Immobilon-P PVDF membranes (Millipore). The membrane was blocked by 5% BSA in TBST (150 mM NaCl, 25 mM Tris-HCl (pH 7.4) supplemented with 0.1% Tween 20) and incubated with rabbit anti-ATF4 polyclonal antibody (1/2,000), followed by HRP-conjugated anti-rabbit IgG (1/10,000). The signals were detected using an ECL chemiluminescence substrate (Amersham Biosciences). The quantitative analysis of blots was normalized using the lumino image analyzer LAS-4000 (Fujifilm Corp., Japan).

Statistics—Data are presented as the mean ± S.E. for the indicated number of independent experiments. Statistical significance was determined with a post-hoc test of one-factor factorial analysis of variance (Figs. 3*E*, 6*D*, 7*B*, and 7*C*), the Wilcoxon Mann-Whitney *U* test (non-parametric analysis, Fig. 2*C*, and Fig. 6*C*), and Student's *t* test (other figures) using the KaleidaGraph® 4.0 programs (Synergy Software, Reading, PA). Differences with a p value of <0.05 was considered statistically significant (* and # indicate up-regulation and down-regulation, respectively; NS indicates not significant).

RESULTS

CCR1-deficient Mice Exhibit Osteopenia—To understand the functions of CCR1 in bone metabolism, we investigated the bone mineral density in $Ccr1^{-/-}$ mice. A peripheral quantitative CT analysis showed a significant reduction in bone mineral

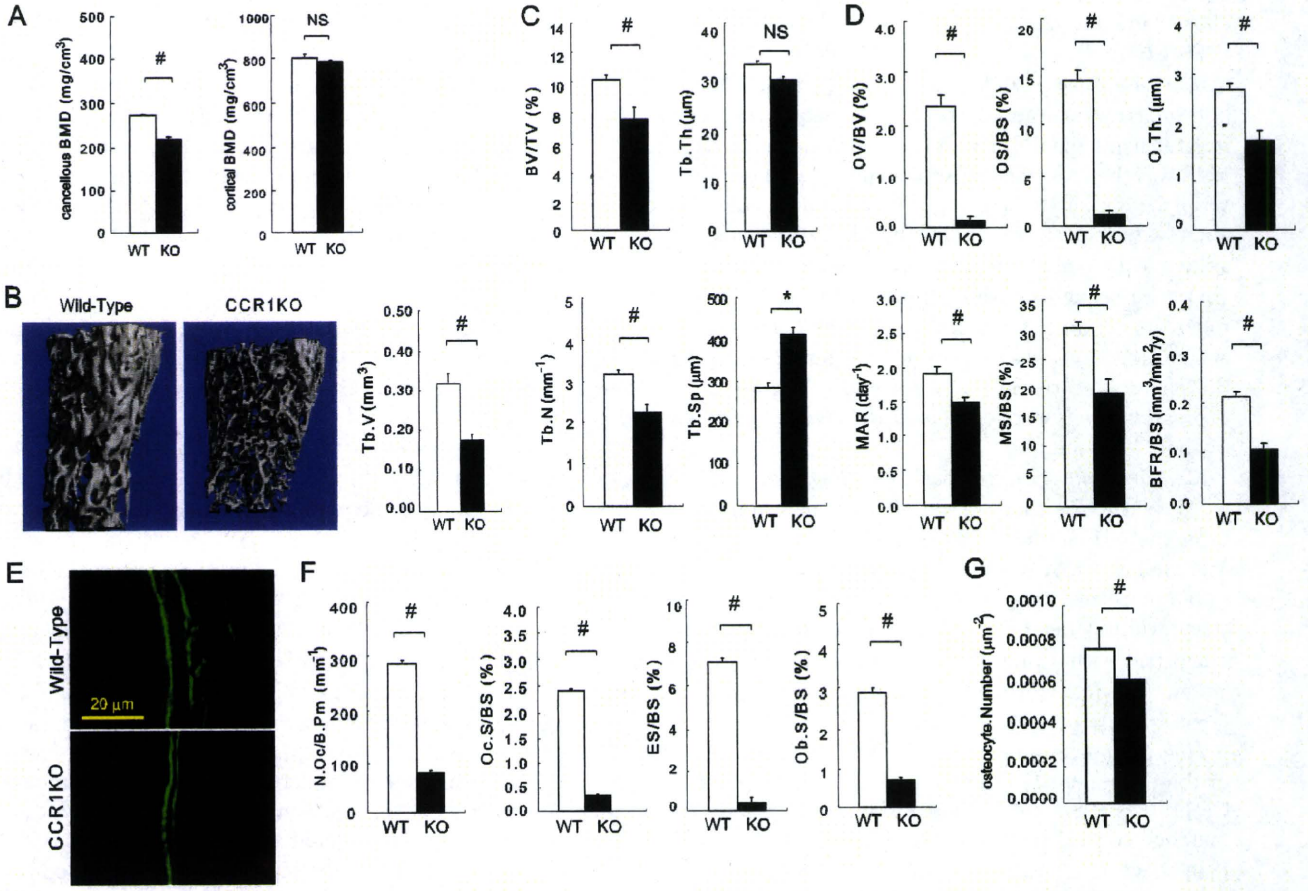

FIGURE 1. **Bone morphometric analyses of CCR1$^{-/-}$ mice.** *A* shows the bone mineral density of trabecular and cortical bones in distal femurs as measured by peripheral quantitative CT. *B* shows the microCT images and the quantitative measurements of trabecular bones (*Tb.V.*) in the distal femurs of wild-type and *Ccr1*$^{-/-}$ mice (n = 10). In *C–F*, the bone histomorphometric analyses of distal femurs in wild-type and *CCR1*$^{-/-}$ mice were carried out as described under "Experimental Procedures." Parameters relating to the trabecular structure (in *C*): bone volume per tissue volume (*BV/TV*), trabecular number (*Tb.N.*), and trabecular separation (*Tb.Sp.*). Parameters relating to bone formation (in *D*): osteoid volume to bone volume (*OV/BV*), osteoid surface/bone surface (*OS/BS*), osteoid thickness (*O.Th.*), formation rate referenced to bone surface (*BFR/BS*), mineral apposition rate (*MAR*), and mineralizing surface per bone surface (*MS/BS*). The immunofluorescence images of calcein labeling in wild-type and *Ccr1*$^{-/-}$ mice (in *E*). Parameters relating to bone resorption (in *F*): osteoclast number per bone perimeter (*N.Oc./B.Pm*), osteoclast surface per bone surface (*Oc.S./BS*), eroded surface per bone surface (*ES/BS*), and osteoblast surface per bone surface (*Ob.S./BS*). The bone histomorphometric analysis data are represented as the mean ± S.E. obtained from six mice in each group. #, significantly different from wild-type controls, $p < 0.05$. In *G*, osteocyte numbers per area are represented as the mean ± S.E. obtained from three mice in each group.

density in cancellous bone in *Ccr1*$^{-/-}$ mice compared with wild-type mice (Fig. 1*A*). There were no significant differences between bone mineral density in the cortical bone at the metaphysial (Fig. 1*A*) and diaphysial regions (data not shown) between *Ccr1*-deficient and wild-type mice. In *Ccr1*$^{-/-}$ mice, a microCT analysis indicated decreased cancellous bone tissue at the metaphysical region (Fig. 1*B*). An analysis of bone histomorphometrics confirmed a significant decrease of bone volume (*BV/TV*) at the metaphysial region of *Ccr1*$^{-/-}$ mice. This was associated with a diminished number of trabeculae (*Tb.N*), increased trabecular bone separation (*Tb.Sp*), and no significant changes in trabecular bone thickness (*Tb.Th*), thus indicating that *Ccr1*-deficient mice have sparse trabeculae (Fig. 1*C*). We examined the effect of *Ccr1* deficiency on the function of osteoblasts and osteoclasts in bone morphometry (Fig. 1, *D–F*). The morphological analyses revealed that *Ccr1*$^{-/-}$ mice have a significantly reduced number of osteoblasts (*Ob.S./BS*) (Fig. 1*F*). *Ccr1*$^{-/-}$ mice exhibited extremely low values of osteoid surface (*OS/BS*) and osteoid volume (*OV/BV*) compared with wild-type mice (Fig. 1*D*). Notably, *Ccr1*$^{-/-}$ mice showed a significant decreases in the mineral apposition rate (*MAR*), mineralized surface (*MS/BS*), and bone formation rate (*BFR/BS*) (Fig. 1*D*), which were calculated based on calcein administration (*representative pictures* are shown in Fig. 1*E*). In addition, the number of osteocytes per area was significantly reduced in *Ccr1*$^{-/-}$ mice (Fig. 1*G*). These results indicate that *Ccr1*$^{-/-}$ mice have impaired bone formation. Fig. 1*F* summarizes the bone morphometric parameters associated with bone resorption. *Ccr1*$^{-/-}$ mice have significantly decreased osteoclast numbers (*N.Oc./B.Pm*) and osteoclast surface area (*Oc.S./BS*), and an eroded surface (*ES/BS*). These findings indicate that *Ccr1*$^{-/-}$ mice have diminished osteoclast function. Taken together, the morphometric analyses suggest that the bone phenotype in *Ccr1*-deficient mice exhibit osteopenia with low bone turnover, which is most likely due to the diminished function of osteoblasts and osteoclasts.

Impaired Osteogenesis and Osteoclastogenesis in the Bone Tissue of Ccr1-deficient Mice—To elucidate the status of osteoblasts and osteoclasts in bones of *Ccr1*$^{-/-}$ mice, we compared the transcriptional levels of osteoclast- and osteoblast-related

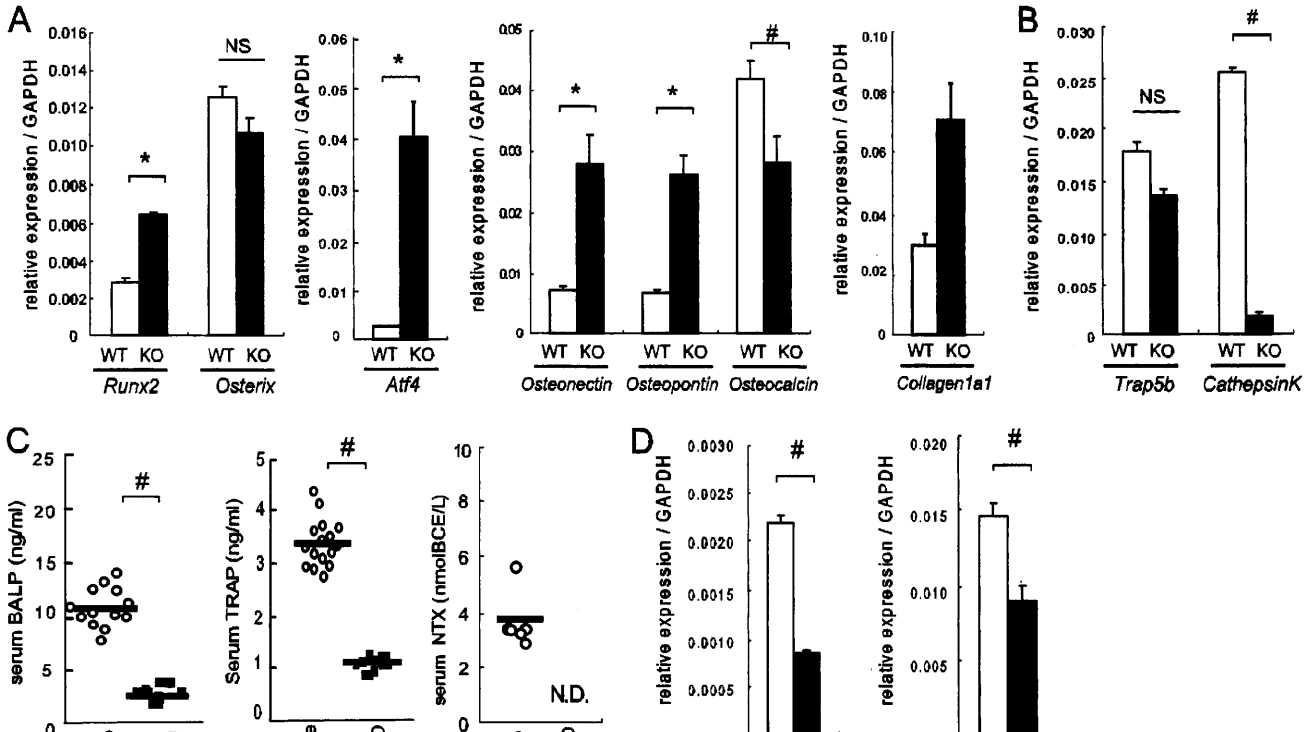

FIGURE 2. **Expression of markers related to osteoblasts and osteoclasts in bones and sera in wild-type and *CCR1*$^{-/-}$ mice.** In *A*, *B*, and *D*, total RNAs were isolated form the proximal tibia of wild-type and *Ccr1*$^{-/-}$ male mice at 8 weeks of age. Real-time Q-PCR revealed the relative expression levels of osteoblast-related mRNAs (*Runx-2*, *Osterix*, *Atf4*, *Osteonectin*, *Osteopontin*, *Osteocalcin*, and *Collagen1α1*, *A*), osteoclast-related mRNA (*Trap5a* and *Cathepsin K*, *B*), and RANK-RANKL axis (*Rank* and *Rankl*, *D*). Data are expressed as the copy numbers of these markers normalized to *Gapdh* expression (mean ± S.E., $n = 8$). In *C*, the levels of serum BALP, TRAP, and *serum* collagen-type1 N-telopeptides (*NTx*) were measured by ELISA. The *bars* indicate the mean ± S.E. Each sample was duplicated. Wild-type and *Ccr1*$^{-/-}$ male mice at 9 weeks of age ($n = 10$ and 6, respectively) were subjected to BALP and TRAP. Wild-type and *Ccr1*$^{-/-}$ male mice at 9–13 weeks of age ($n = 8$ and 6, respectively) were assayed for NTx. #, significantly different from wild-type controls, $p < 0.05$. *N.D.*, not detected.

markers in the proximal tibiae of wild-type and *Ccr1*$^{-/-}$ mice. The analyses of osteoblast-related markers, such as bone-specific transcriptional factors (*Runx-2*, *Atf4*, and *Osterix*) (23–25) and bone matrix proteins (*Collagen1a1*, *Osteonectin*, *Osteopontin*, and *Osteocalcin*), revealed that the expression levels of *Runx2* and *Atf4* were dramatically up-regulated in *Ccr1*$^{-/-}$ mice than in wild-type mice (Fig. 2*A*). However, there were no significant changes in the expression levels of *Osterix*. Early markers for osteoblast differentiation, including *Collagen1a1*, *Osteonectin*, and *Osteopontin*, were significantly up-regulated. *Osteocalcin* expression, a marker for mature osteoblasts, was significantly down-regulated in *Ccr1*$^{-/-}$ mice. These results suggest that osteoblasts in *Ccr1*-deficient mice are retained in an immature state due to the overexpression of *Runx-2* and *Atf4* by osteoblasts, which is also consistent with the significant reduction in number of osteocytes in *Ccr1*$^{-/-}$ mice. Constitutive *Runx-2* overexpression in osteoblasts results in maturation arrest in osteoblasts and in a reduced number of osteocytes (25). The serum levels of BALP in *Ccr1*-deficient mice were significantly decreased (Fig. 2*C*).

The expression levels of markers related to osteoclast differentiation, revealed attenuated transcription levels of *TRAP5b* and *cathepsin K* in *Ccr1*$^{-/-}$ mice (Fig. 2*B*). In addition, *Ccr1*$^{-/-}$ mice exhibited significantly decreased levels of serum TRAP (26) and collagen-type I *NTx* (*27, 28) (Fig. 2C*). This finding is consistent with diminished osteoclastic bone resorption in *Ccr1*$^{-/-}$ mice. These observations led us to assess the RANK-RANKL axis, a key signaling pathway in osteoblast-osteoclast interactions that regulates osteoclast differentiation and function. Interestingly, the analyses revealed that both *Rank* and *Rankl* were down-regulated (Fig. 2*D*), thus implying that CCR1 is involved in the regulation of the RANK-RANKL axis. Considering the fact that *Ccr1*$^{-/-}$ mice exhibit osteopenia with low bone turnover, these bone cell marker expression levels suggest that CCR1 is heavily involved in the differentiation and function of osteoblasts and osteoclasts as well as in the cellular interactions between these cell types.

CCR1 Signaling Is Important in the Maturation and Function of Osteoblasts—To further corroborate the necessity of CCR1 in osteoblast maturation and function, we examined the formation of mineralized nodules *in vitro* by osteoblastic cells isolated from bone marrow of wild-type and *Ccr1*$^{-/-}$ mice. Mineralized nodule formation in osteoblastic cells isolated from *Ccr1*$^{-/-}$ mice was markedly abrogated compared with wild-type osteoblastic cells (Fig. 3*A*). We next investigated the time-course expression profiles of osteoblastic markers in this *in vitro* culture system and compared them between wild-type and *Ccr1*$^{-/-}$ mice (Fig. 3*B*). In wild-type mice, *Runx2* exhibited the highest levels of expression at day 14, but was drastically down-regulated at day 21, during the mineralization stage. However,

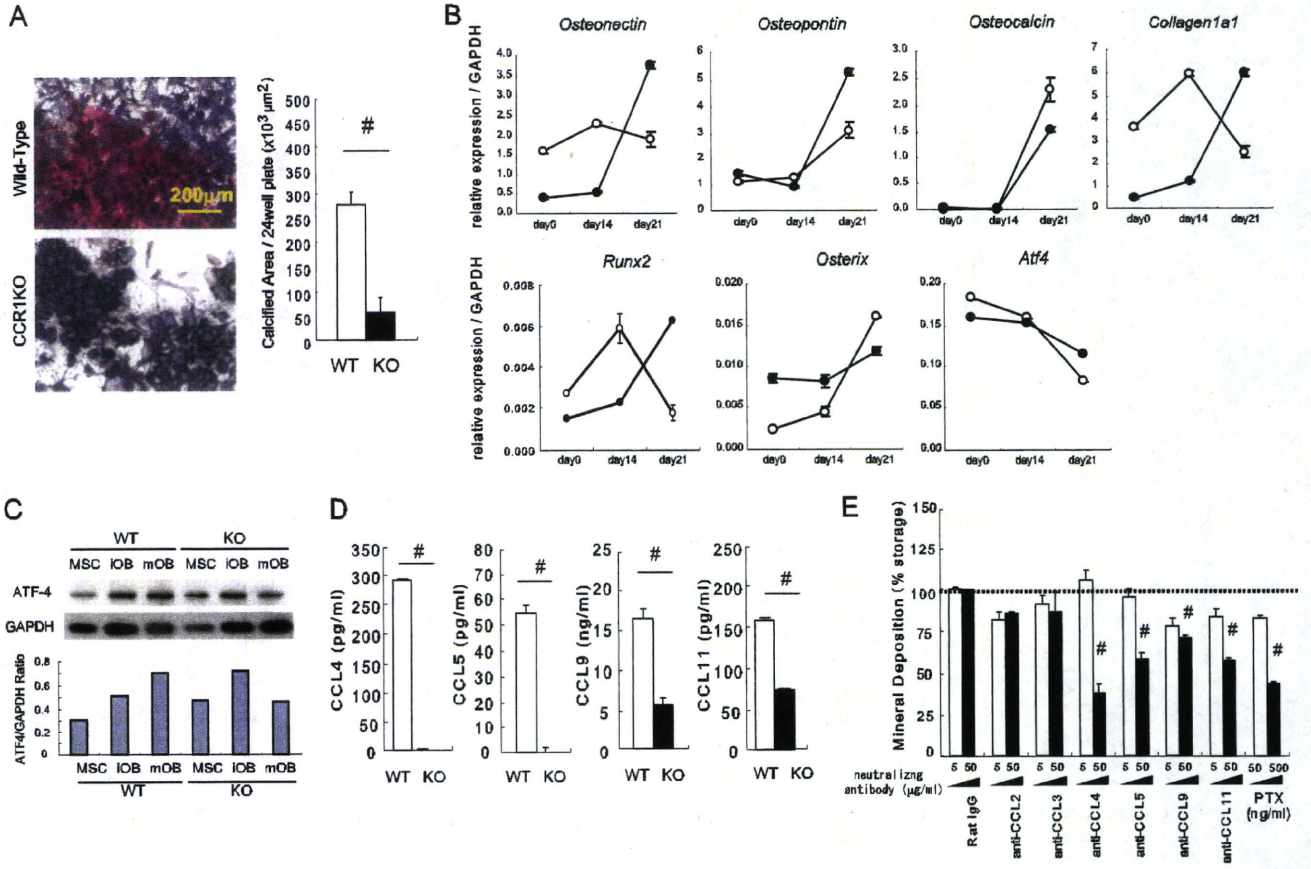

FIGURE 3. **Impaired mineralized nodule formation in *CCR1*-deficient osteoblastic cells.** In *A*, osteoblastic cells were cultured from the bone marrow of wild-type and *Ccr1*$^{-/-}$ mice, and then minerals were stained with alizarin red and BALP with chromogenic reagents (shown in "*blue*") (magnification ×100, *left*). Mineral deposition was determined by von Kossa staining ($n = 6$, *right*). In *B*, total RNAs were isolated from osteoblastic cells isolated from wild-type (*open circles*) and *Ccr1*$^{-/-}$ mice (*filled circles*). The real-time Q-PCR analyses examined the relative expression levels of osteoblast-related transcriptional factor mRNAs (*Runx-2*, *Osterix*, and *Atf4*) and osteoblast-related marker mRNAs (*Osteonectin*, *Osteopontin*, *Osteocalcin*, and *Collagen1α1*). Data are expressed as the copy numbers of these markers normalized to *Gapdh* expression (mean ± S.E., $n = 8$). In *C*, the protein expression levels of the transcriptional factor ATF4 by wild-type and *Ccr1*$^{-/-}$ osteoblastic cells were measured by a Western blot analysis. Osteoblast lysates (10 μg of protein per lane) was loaded and separated by SDS-PAGE. The expression levels of ATF4 were normalized to GAPDH expression. In *D*, the production of CCR1-related chemokine ligands in the culture media of wild-type and *Ccr1*$^{-/-}$ osteoblastic cells was measured by ELISA ($n = 5$). #, significantly different from wild-type controls, $p < 0.05$. In *E*, osteoblastic cells were cultured with the indicated neutralizing antibodies against chemokines. The mineral deposition rate was measured by von Kossa staining ($n = 4$). Stained cells cultured with control rat IgG were set as 100%. #, significantly different from between different concentrations of each antibody, $p < 0.05$. *PTX*, pertussis toxin.

an inverse *Runx2* expression pattern was observed in CCR1-deficient osteoblastic cells, in which the levels of expression were markedly suppressed in the early stages (days 0 and 14), and was then significantly up-regulated at day 21, reaching the levels present in wild-type mice. *Osterix* expression was highly up-regulated at day 21 in wild-type mice, whereas its expression in CCR1-deficient osteoblastic cells was sustained at an intermediate level between the lowest and the highest levels in wild-type mice, overall resulting in a lower expression levels than in wild-type mice at day 21. These inverted expression patterns were also consistently observed, especially at day 21, with other osteoblastic markers, including *Atf4*, *Caollagen1a1*, *Osteonectin*, *Osteopontin*, and *Osteocalcin*. Similarly, the expression pattern of ATF4 was also confirmed by a Western blot analysis (Fig. 3*C*). These observations indicated that CCR1 deficiency severely affected the temporal expression of osteoblastic markers, resulting in the impaired differentiation and maturation of osteoblasts. Because CCR1 signaling is activated by several cross-reactive chemokines (CCL4, CCL5, CCL9, and CCL11), we next compared the levels of these chemokines in wild-type and CCR1-deficient osteoblastic cells. We observed significantly diminished expression levels of these chemokines in *CCR1*-deficient osteoblastic cells (Fig. 3*D*). A test on the effects of neutralizing antibodies against various chemokines, including CCR1 ligands, revealed the role of each chemokine in mineralized nodule formation by osteoblastic cells. The neutralizing antibodies against CCL4, CCL5, CCL9, and CCL11 significantly reduced the number of mineralized nodules in osteoblastic cells, although the antibodies against CCL2 and CCL3 did not inhibit the numbers completely (Fig. 3*E*). Pertussis toxin (PTX), an inhibitor of G_i protein-coupled receptors involved in chemokine signaling, inhibited mineralized nodule formation in a dose-dependent manner. In further support of these findings, we observed similar temporal changes in the transcriptional levels of osteoblastic markers in wild-type osteoblastic cultures treated with an anti-CCL9 antibody, compared with *Ccr1*$^{-/-}$ osteoblastic cells (supplemental Fig. 2). These results suggest that CCR1 signaling mediated by its ligands (CCL4, CCL5, CCL 9, and CCL11) plays an essential role in mineralized nodule formation.

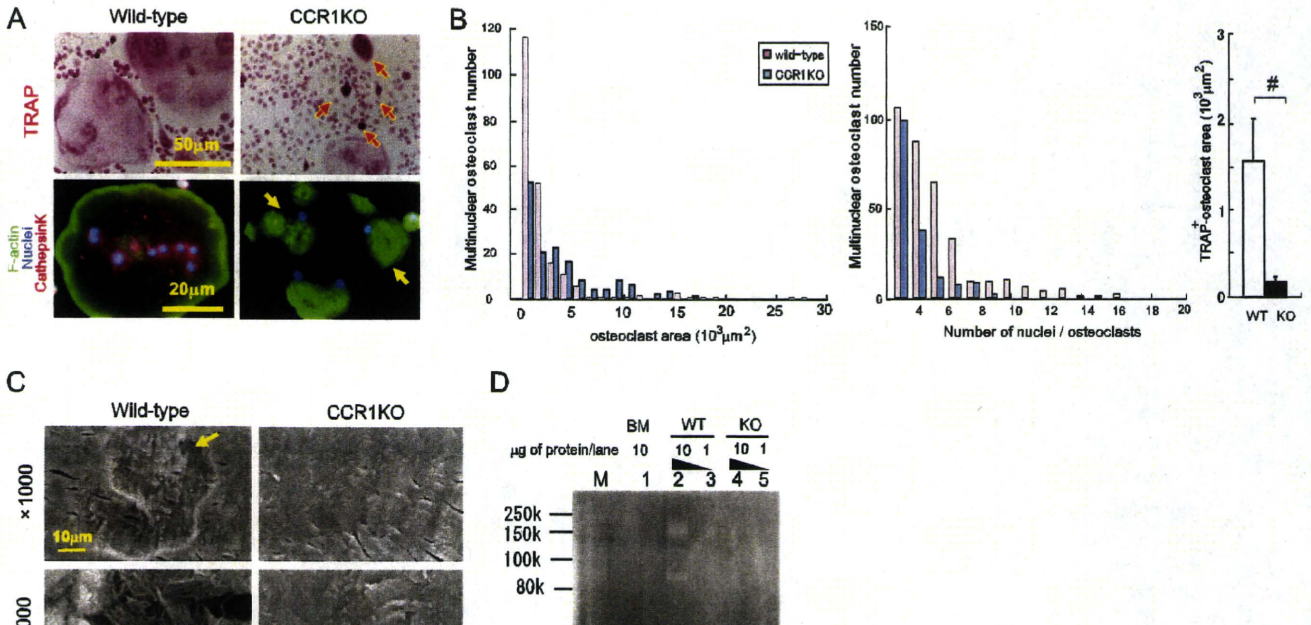

FIGURE 4. **Essential roles of CCR1 in multinucleation and bone-resorbing activity.** Pre-osteoclastic cells were cultured from the bone marrow of wild-type and *Ccr1*$^{-/-}$ mice. Osteoclasts were induced from the pre-osteoclastic cells by M-CSF and RANKL treatment. In *A*, the formation of multinuclear osteoclasts by wild-type and *Ccr1*$^{-/-}$ precursors was visualized by TRAP chromogenic staining (magnification ×400, *upper panels*). Immunohistochemical staining was carried out using an anti-cathepsin K antibody conjugated with Alexa594 (*red*). F-actin and nuclei were counterstained by phalloidin-AlexaFluor 488 (*green*) and Hoechst 33258 (*blue*), respectively (magnification ×640, *bottom panels*). The *yellow arrow* indicates multinuclear giant cells with an impaired actin ring rearrangement, and the *red arrows* indicate TRAP accumulation. In *B*, *histograms* of the area distribution of multinuclear osteoclasts delimited with phalloidin, and of the number of multinuclear osteoclasts in *A*. Area comprises TRAP-positive multinuclear (>3 nuclei) giant cells shown in *A* (mean ± S.E., $n = 3$). In *C*, pit formation by wild-type and *Ccr1*$^{-/-}$ osteoclasts on bone slice observed by scanning electron microscopy (magnification: ×1000 (*top*) and ×6000 (*bottom*), respectively). In *D*, collagen digestion activity by wild-type and *Ccr1*$^{-/-}$ osteoclasts was measured by collagen-based zymography. *Lanes M*, *1*, *2–3*, and *4–5* indicate the molecular markers, bone marrow-derived macrophage lysates (10 μg of protein/*lane*), wild-type osteoclast lysates (1 and 10 μg of protein/*lane*), and *Ccr1*$^{-/-}$ osteoclasts lysates (1 and 10 μg of protein/each *lane*), respectively.

Lack of Chemokine Receptor CCR1 Causes Impaired Osteoclast Differentiation and Bone-resorbing Activity—To elucidate the roles of CCR1 in osteoclast differentiation, we analyzed the differentiation potency of osteoclast precursors derived from *Ccr1*$^{-/-}$ mice (Fig. 4*A*). Osteoclast precursors from *Ccr1*-deficient mice markedly abrogated multinucleation with defective actin ring formation (Fig. 4*A*, *yellow arrows*) compared with precursors from wild-type mice, which generated a large numbers of osteoclasts with multinucleation and well organized actin ring formation at the cell periphery. The histograms of the osteoclast area and number of nuclei per cell as well as TRAP-positive areas reveal the presence of impaired cellular fusion and differentiation in *Ccr1*-deficient osteoclasts (Fig. 4*B*). We further investigated the activity of bone resorption in *Ccr1*-deficient osteoclasts (Fig. 4*C*). Few resorption pits were observed in *Ccr1*$^{-/-}$ osteoclasts by scanning electron microscopic examination, in contrast to obvious resorption pits with well digested collagen fibers detected in wild-type osteoclasts. This observation was also confirmed by collagen zymography demonstrating that *Ccr1*$^{-/-}$ osteoclasts failed to digest type-I collagens (Fig. 4*D*).

Furthermore, the transcriptional levels of osteoclastic differentiation markers were investigated in the osteoclast culture system. *Rank* and its downstream targets *Nfat-c1*, other markers such as *c-fos*, *Trap*, *CathepsinK*, *Atp6v0d2*, *integrin αV*, and *integrin β3* were markedly down-regulated in *Ccr1*-deficient cells, whereas *S1P*$_1$ and *Irf-8* were up-regulated (Fig. 5*A*). We next examined whether the down-regulation in RANK expression *in vivo* (see Fig. 2*D*) and *in vitro* (Fig. 5*A*) directly correlated with the reduction in RANK-expressing osteoclast precursors. The cellular profiles of osteoclast precursors by a flow cytometric analysis revealed that the *Ccr1*$^{-/-}$ mice had lower numbers of CD45$^+$CD11b$^+$CD115$^+$ myeloid-lineage precursors compared with wild-type mice (Fig. 5*B*). In addition, the subpopulations of osteoclast precursors, which are categorized into CD11b^{hi} (R1) and CD11b^{lo} (R2), were marked reduced in the R2 subpopulation in CCR1-deficient cells. Because the R1 and R2 subpopulations reportedly express higher and lower levels of RANK, respectively (29), a reduction in the R2 subpopulation likely contributed to reduced expression of osteoclast markers in CCR1-deficient osteoclastic cells. Importantly, our observation is also consistent with a previous work reporting that RANK^{lo} precursors are required for cellular fusion (29).

CCR1 Signaling Is Involved in Osteoclast Differentiation—To further explore the role of CCR1 signaling in osteoclast differentiation, we next examined the expression levels of chemokine receptors during osteoclastogenesis using an *in vitro* culture system. CCR1 was expressed in the course of the osteoclastogenesis, with the highest levels of expression at day 4 after culture (10–12), whereas other chemokine receptor CCR2 was gradually down-regulated during this culture period (30)

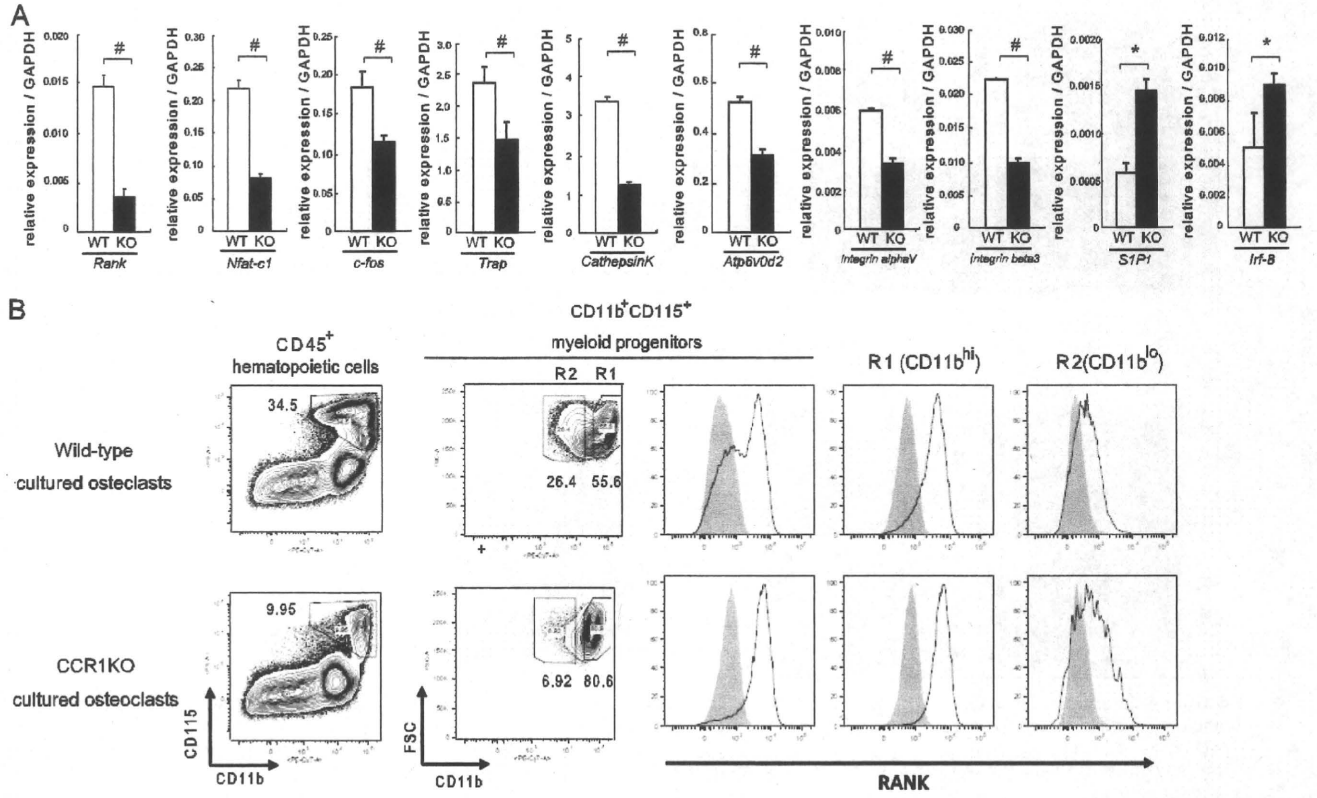

FIGURE 5. **Osteoclastic impairment by CCR1 deficiency is due to the changes in osteoclastic precursor population.** Pre-osteoclastic cells were cultured from the bone marrow of wild-type and *Ccr1*$^{-/-}$ mice. Osteoclasts were induced from the pre-osteoclastic cells by M-CSF and RANKL treatment. In *A*, relative expression levels of the osteoclastic differentiation markers (*Rank*, *Nfatc1* transcription factor, *c-fos*, *Trap*, *CathepsinK* protease, H$^+$-ATPase subunit *ATP6v0d2*, integrins αV and $\beta 3$, *S1P*$_1$, and *Irf-8*) on wild-type (*open column*) and *Ccr1*$^{-/-}$ (*filled column*) osteoclasts were measured by a real-time Q-PCR analysis at day 4 after culture (mean ± S.E., $n = 5$). #, significantly different from wild-type controls, $p < 0.05$. In *B*, expression analysis of RANK in CD45$^+$CD11b$^+$CD115$^+$ pre-osteoclastic cells isolated from the bone marrows of wild-type and *Ccr1*$^{-/-}$ mice after 4 days in culture were analyzed by flow cytometry.

(Fig. 6*A*). Immunohistochemical staining revealed that CCR1 was highly expressed on the multinuclear osteoclasts (supplemental Fig. 3). The expression profiles of CCR ligands in this *in vitro* osteoclast culture system revealed that ligands specific for CCR1, such as *Ccl5* and *Ccl9*, had a relatively higher levels of expression than other ligands, and appeared to be regulated depending on the maturation stages of the osteoclasts. *Ccl5* was preferentially expressed at day 4, a stage of mononuclear pre-osteoclasts, whereas multinuclear osteoclasts predominantly produced *Ccl9* at later times (Fig. 6*B*). These regulated transcriptional patterns of *Ccl5* and *Ccl9* were also confirmed by the analysis of protein expression levels in cultured media (Fig. 6*C*). These observations suggested that the interaction between CCR1 and its ligands, CCL5 and CCL9, could be involved in osteoclast differentiation.

We verified this hypothesis by culturing osteoclast precursors in the presence of neutralizing antibodies against CCL5 and CCL9. Blockade of either ligand resulted in a partial inhibition of osteoclast formation in a dose-dependent manner. Similarly, simultaneous treatment with neutralizing antibodies against CCL5 and CCL9 induced synergistic inhibitory effects (Fig. 6*D*). Furthermore, PTX treatment blocked osteoclastogenesis to the basal levels. Notably, we found no CCL3 production by ELISA or any inhibitory osteoclastogenesis effects using an anti-CCL3 antibody (data not shown), although CCL3 is thought to play an essential role in inflammation-related osteoclastogenesis in humans (4, 7, 31, 32). These findings indicate that CCR1 is essential for osteoclast differentiation, and CCL5 and CCL9 are the likely candidate ligands that participate in the CCR1 axis.

CCR1 Is Involved in the RANK–RANKL Axis and Induces the Impaired Osteoclastogenesis—Because osteoclast differentiation is critically regulated by the signals through the RANK–RANKL axis, we investigated the transcriptional level of *Rankl* in *Ccr1*$^{-/-}$ osteoblastic cells. The cells expressed significantly lower levels of RANKL compared with wild-type osteoblastic cells (Fig. 7*A*). We next performed co-cultures of pre-osteoclasts with layers of osteoblastic cells by reciprocal combinations of these two cell populations from wild-type and *Ccr1*$^{-/-}$ mice. As expected from the reduced *Rankl* expression, a significantly reduced number of osteoclasts were formed from co-culture with *Ccr1*$^{-/-}$ osteoblastic cells compared with wild-type osteoblastic cells (Fig. 7*B*). In the presence of PTX, wild-type osteoblastic cells also failed to generate substantial numbers of osteoclasts (Fig. 7*B*). *Ccr1*$^{-/-}$ osteoclast precursors did not form differentiated osteoclasts even in the presence of wild-type-derived osteoblasts (Fig. 7*C*), as is consistent with our observations in Fig. 4. These observations suggest that the CCR1 chemokine receptor, which is expressed by both osteoblasts and osteoclasts, plays a critical role on osteoblast-osteoclast communication through the regulation of the RANK and RANKL expression.

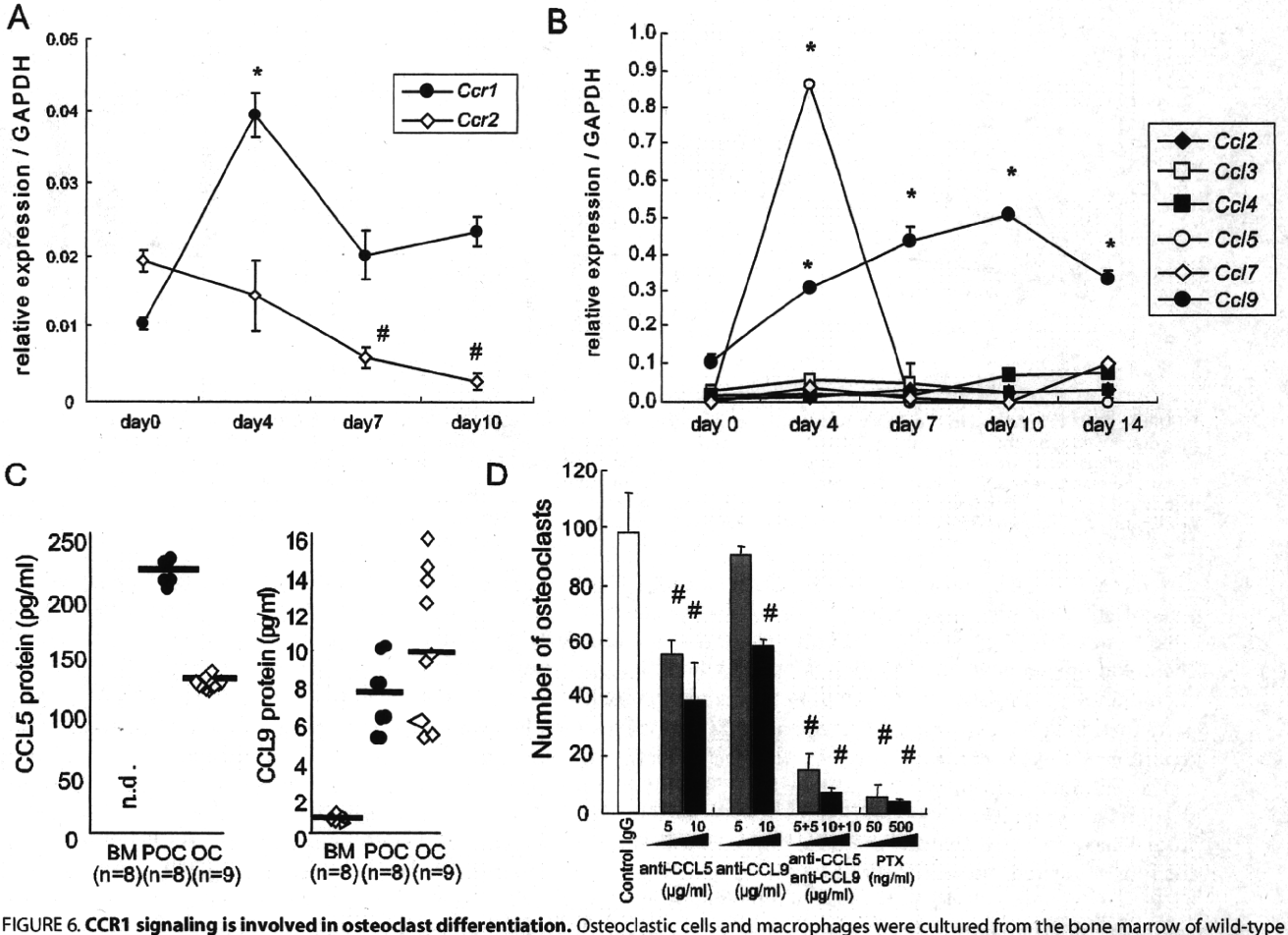

FIGURE 6. **CCR1 signaling is involved in osteoclast differentiation.** Osteoclastic cells and macrophages were cultured from the bone marrow of wild-type and *Ccr1*$^{-/-}$ mice. Total RNAs were isolated from the cultured cells. The relative mRNA expression levels of chemokine receptors *Ccr1*, *Ccr2* (*A*) and chemokine ligands (*B*) during osteoclastogenesis were measured by real-time Q-PCR (mean ± S.E., $n = 5$). * and #, significantly different from day 0 of *Ccr1* and *Ccr2*, respectively, $p < 0.05$ in *A*. *, significantly different from day 0 of culture in each ligand expression, $p < 0.05$ in *B*. In *C*, chemokine levels during osteoclastogenesis were measured by ELISA. *BM*, bone marrow-derived macrophage; *POC*, pre-osteoclast (day 4); and *OC*, osteoclast (day14). *Bars* indicate the mean. In *D*, the number of osteoclasts after neutralization of CCL5, CCL9, and their combination in the osteoclastic cultures were scored (mean ± S.E., $n = 3$). #, significantly different between two distinct concentrations of each antibody, $p < 0.05$. *PTX*, pertussis toxin.

DISCUSSION

Pathological findings postulate that chemokines and chemokine receptors are involved in bone remodeling (9–13). Among these receptors, CCR1 appears to be an important molecule involved in bone metabolism (9). We used *Ccr1*$^{-/-}$ mice to investigate whether CCR1 affects bone metabolism. Our findings have demonstrated that a CCR1-deficiency affects the differentiation and function of both osteoblasts and osteoclasts, and also causes osteopenia.

Our bone histomorphometric study in *Ccr1*$^{-/-}$ mice clearly demonstrated impaired osteoblast differentiation and function (Fig. 1, *D–G*). The bone tissues in *Ccr1*$^{-/-}$ mice exhibited down-regulation of *osteocalcin*, which is a marker for mature osteoblasts, whereas the expression of *Osteonectin* and *Osteopontin*, which are markers for early osteoblasts, were up-regulated in the bones of these mice (Fig. 2*A*). Significantly, *Ccr1*$^{-/-}$ osteoblastic cells exhibited much less potency to generate mineralized tissues (Fig. 3*A*). These results suggest that the deficiency of CCR1 results in arrested osteoblast maturation and defective osteoblast function. Previous reports have demonstrated that the sustained expression of *Runx2* in osteoblasts inhibits their terminal maturation and causes osteopenia with a reduction in the number of osteocytes (25, 33). Consistent with these findings, bone tissue specimens from *Ccr1*$^{-/-}$ mice exhibited a higher expression level of *Runx2* and a reduced number of osteocytes (Fig. 3*G*). These findings suggest that osteopenia in *Ccr1*$^{-/-}$ mice is due to impaired osteoblastic function via *Runx2* up-regulation. Our findings in *Ccr1*$^{-/-}$ osteoblastic culture supportively demonstrated that an inverse temporal expression level of osteoblastic transcriptional factors, such as *Runx2*, *Atf4*, and *Osterix* could be related to the disordered expressions of bone matrix proteins, thus resulting in impaired bone mineral deposition (Fig. 3*B*).

Furthermore, treatment with neutralizing antibodies against CCR1 ligands (*e.g.* CCL4, CCL5, CCL9, and CCL11) significantly inhibited mineral deposition (Fig. 3*E*) and osteoblastic protein expression (supplemental Fig. 2) in osteoblastic cells isolated from wild-type mice. These observations indicate that CCR1-mediated signaling is essential for osteoblast differentiation and function. Although we detected substantial levels of

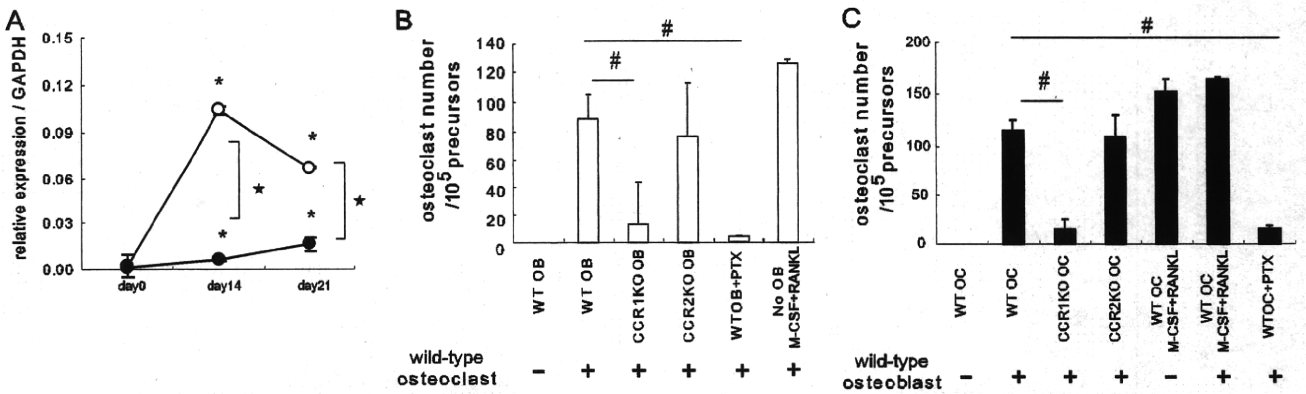

FIGURE 7. **CCR1 is involved in the RANK–RANKL axis and induces the impaired osteoclastogenesis.** In *A*, osteoblastic cells were cultured from the bone marrow of wild-type and *Ccr1*$^{-/-}$ mice. Relative expression levels of *Rankl* by *Ccr1*$^{-/-}$ osteoblasts as measured by real-time Q-PCR (mean ± S.E., $n = 3$). #, significantly different from wild-type controls, $p < 0.05$. In *B* and *C*, the number of TRAP$^+$ multinuclear osteoclasts induced by co-culture with osteoblasts. Co-culture with osteoblastic cells isolated from wild-type or *Ccr1*$^{-/-}$ mice (mean ± S.E., duplicated, $n = 2$, *B*), and with osteoclast precursors isolated from wild-type or *Ccr1*$^{-/-}$ mice (mean ± S.E., duplicated, $n = 2$, *C*). Osteoclast cultures with M-CSF and RANKL without osteoblasts were set as positive control. #, significantly different from co-culture of osteoclasts with wild-type osteoblasts, $p < 0.05$.

various chemokine ligands (CCL4, CCL5, CCL9, and CCL11) in osteoblastic cells, these levels were greatly reduced in cells isolated from *Ccr1*$^{-/-}$ mice (Fig. 3*D*). This observation implies a chemokine-dependent amplification loop by which a given chemokine signaling sustains or amplifies the expressions of its participating ligands and receptors, which has been previously reported in several contexts. For instance, the activation of CD14$^+$ monocytes form a CCR2-CCL2 axis-dependent amplification loop that ultimately leads to fibrosis (34). Several other studies have reported that macrophage infiltration in injured tissue is mediated by a CCR1-mediated loop (35–37) and a CCR5–CCL5 loop (38). Reports of renal inflammatory signals and abdominal inflammation have described CCR7–CCL19/CCL21 (39) and CCR8–CCL1 loops (17), respectively. Therefore, the CCR1-mediated loop is likely to be involved in osteoblast differentiation, function, and cellular interactions that regulate bone metabolism. Possible roles of the CCR1-mediated loop in osteoblast differentiation and function suggest that changes in the bone marrow microenvironment by a CCR1 deficiency affected the osteoblastic lineage and/or the intercellular regulation of osteoblast differentiation and function. CCR1 conventional knock-down seems to have affected many cell types that express CCR1, affecting the bone marrow microenvironment, which regulates whole process of osteoblast differentiation and function. Our *in vitro* experiments did not successfully retrieve this point. Nevertheless, the present experiments have confirmed an essential role for CCR1-mediated signaling in osteoblastic cells. The expression and possible roles of CCR1 in osteoclast lineage cells have been reported by several studies (4, 10, 11). We observed the up-regulation of *Ccr1* expression and down-regulation of *Ccr2* during cultured osteoclastogenesis (Fig. 6*A*). The bone histomorphometric analyses demonstrated impaired osteoclast differentiation and function in *Ccr1*$^{-/-}$ mice (Fig. 1*F*). In addition, we observed impaired bone resorption activity by osteoclasts isolated from *CCR1*$^{-/-}$ mice (Fig. 4, *B* and *C*). A potential reason for the impaired bone resorption is due to defects in osteoclast differentiation. Indeed, the flow cytometric analyses revealed that the component of CD11b$^+$CD115$^+$ myeloid-lineage precursors in *Ccr1*$^{-/-}$ mice are drastically changed; this population of cells lacked the RANK^{lo} CD11b^{lo} subpopulation, which is required for cellular fusion (29) (Fig. 5*B*). Recent live observation of calvarial bone marrow by two-photon microscopy clarified the roles of chemoattractant S1P$_1$ (sphingosine-1-phosphate 1) and its receptors in the migration of osteoclast precursors to the bone surface (40). Therefore, it is indeed intriguing to speculate that elevated levels of *S1P$_1$* expression in *Ccr1*$^{-/-}$ osteoclasts (Fig. 1*F*) reduced the supply of osteoclast precursors from peripheral circulation in the bone marrow to the bone surface. Further investigation will reveal whether the CCR1 axis is involved in the chemotactic migration of osteoclast precursors to the bone surface.

One of the possible reasons for osteoclast dysfunction in *Ccr1*$^{-/-}$ mice may be diminished signaling along the RANK–RANKL axis. The down-regulation of both *Rank* and *Rankl* mRNA was observed in the bone tissue of *Ccr1*$^{-/-}$ mice (Fig. 2*D*). Cultured osteoblastic cells and osteoclasts isolated from *Ccr1*$^{-/-}$ mice exhibited remarkable reductions in *Rank* and *Rankl* expression levels, respectively (Figs. 5*B* and 7*B*). Furthermore, *Ccr1*-deficient osteoclasts had discouraged the levels of osteoclastic maturation markers such as c-*fos*, *Nfatc1*, *CathepsinK*, and several integrins (Fig. 5*A*). These results suggest that CCR1-mediated signaling controls the RANK–RANKL axis through the regulation of both osteoblasts and osteoclasts. Our intercross co-cultures of pre-osteoclasts with osteoblastic cells from wild-type and *Ccr1*$^{-/-}$ mice obviously demonstrated an impaired interaction between these two cell types, resulting in the impaired induction of functional mature osteoclasts (Fig. 7, *B* and *C*). These findings, interestingly, support the idea that the chemokines produced by the osteoblasts and osteoclasts that stimulate CCR1-mediated signaling could be categorized as putative "bone-coupling factors" (41), which mediate the cross-talk between osteoclasts and osteoblasts to maintain bone remodeling.

Our data imply that the regulatory mechanism of *Rankl* expression is associated with osteoblast maturation. Runx2 reportedly induce a low steady-state level of *Rankl* expression and is also required for the stimulatory effect of vitamin

D_3 on *Rankl* transcription possibly by condensing or decondensing the chromatin structure (42). It is possible that the inverse-temporal *Runx2* expression in CCR1-deficient mice is causative of the down-regulation of *Rankl*, due to a reduced cellular response to bone-targeted hormones such as vitamin D_3 and parathyroid hormone. However, a more direct role of CCR1-mediated signaling on *Rankl* transcription remains to be elucidated.

CCR1-mediated signaling pathways on both osteoblasts and osteoclasts raise important questions on how the several members of murine chemokine ligands for CCR1 (in rodents, CCL3, CCL4, CCL5, CCL6, CCL8, CCL9, and CCL11) (43) distinguish the downstream signaling pathways, despite sharing the same CCR1 receptor. Each chemokine may possess specific regulatory control for binding to the receptor and inducing a specific cellular response. For example, the osteoclasts may have a distinct intrinsic signaling adaptor protein for cellular response, as well as the adaptor protein FROUNT for CCR2-mediated signaling (44). It has also been demonstrated that the spatiotemporal expression of chemokine receptors and their ligands may relay chemokine signaling and sequential output that regulate bone metabolism. This is related to several findings in this study, including the distinct temporal expression patterns of different ligands as observed in Fig. 6 (*B* and *C*) and supplemental Fig. 1, the chemokine-dependent amplification loop, and the possible chemokine-mediated cellular interaction. Further studies are warranted to investigate the intracellular signaling pathways downstream of each chemokine receptor.

Our current results also support the concept that chemokine receptor antagonists are potentially novel therapeutic candidates for the treatment of patients with certain inflammatory bone diseases. Several reports suggest that CCL3 promotes pathological bone destruction by excessively triggering osteoclast activation (2, 4, 7, 31, 32). However, we were unable to detect increased CCL3 production by cultured osteoclasts (Fig. 6, *B* and *C*, and data not shown), suggesting that physiological osteoclastogenesis is primarily maintained by CCL9 rather than CCL3. It is probable that pro-inflammatory CCL3 overcomes the physiological process of osteoclastogenesis by CCL9 expression and signaling, thereby inducing ectopic osteoclastogenesis that causes bone destruction mediated by T-lymphocyte-mediated activation (45). Alternatively, the species differences between rodents and humans must be considered; CCL9 is described only in rodents, and the putative human homologue is predicted to be CCL15 and CCL23 (46), which are potent osteoclastogenesis mediators in humans (47). It is therefore worthwhile to dissect the distinct roles of chemokine signaling in both the pathological and physiological contexts, which would provide novel information that may help researchers identify new therapeutic targets.

In conclusion, the present observations provide the first evidence for the physiological roles of CCR1-mediated chemokines in the bone metabolism. Further studies on chemokine receptors in the bone metabolism will enable the targeted development of new therapeutic strategies for the treatment of patients with bone destruction diseases and osteoporosis.

Acknowledgments—We thank Dr. Taeko Dohi, Dr. Harumi Suzuki, Dr. Yasuhiro Natori, and Mikiko Uwano (International Medical Center of Japan (IMCJ)), Dr. Philip M. Murphy (NIH), Dr. Tomoki Nakashima (Tokyo Medical and Dental University), and T. Sakai for valuable advices and supports. The authors are grateful to Dr. Takuro Shimbo and Dr. Tetsuya Mizoue (IMCJ) for statistical support.

REFERENCES

1. Charo, I. F., and Ransohoff, R. M. (2006) *N. Engl. J. Med.* **354,** 610–621
2. Oba, Y., Lee, J. W., Ehrlich, L. A., Chung, H. Y., Jelinek, D. F., Callander, N. S., Horuk, R., Choi, S. J., and Roodman, G. D. (2005) *Exp. Hematol.* **33,** 272–278
3. Kim, M. S., Magno, C. L., Day, C. J., and Morrison, N. A. (2006) *J. Cell Biochem.* **97,** 512–518
4. Menu, E., De Leenheer, E., De Raeve, H., Coulton, L., Imanishi, T., Miyashita, K., Van Valckenborgh, E., Van Riet, I., Van Camp, B., Horuk, R., Croucher, P., and Vanderkerken, K. (2006) *Clin. Exp. Metastasis* **23,** 291–300
5. Haringman, J. J., Smeets, T. J., Reinders-Blankert, P., and Tak, P. P. (2006) *Ann. Rheum. Dis.* **65,** 294–300
6. Choi, S. J., Cruz, J. C., Craig, F., Chung, H., Devlin, R. D., Roodman, G. D., and Alsina, M. (2000) *Blood* **96,** 671–675
7. Han, J. H., Choi, S. J., Kurihara, N., Koide, M., Oba, Y., and Roodman, G. D. (2001) *Blood* **97,** 3349–3353
8. Vallet, S., Raje, N., Ishitsuka, K., Hideshima, T., Podar, K., Chhetri, S., Pozzi, S., Breitkreutz, I., Kiziltepe, T., Yasui, H., Ocio, E. M., Shiraishi, N., Jin, J., Okawa, Y., Ikeda, H., Mukherjee, S., Vaghela, N., Cirstea, D., Ladetto, M., Boccadoro, M., and Anderson, K. C. (2007) *Blood* **110,** 3744–3752
9. Yang, M., Mailhot, G., MacKay, C. A., Mason-Savas, A., Aubin, J., and Odgren, P. R. (2006) *Blood* **107,** 2262–2270
10. Yu, X., Huang, Y., Collin-Osdoby, P., and Osdoby, P. (2004) *J. Bone Miner. Res.* **19,** 2065–2077
11. Lean, J. M., Murphy, C., Fuller, K., and Chambers, T. J. (2002) *J. Cell Biochem.* **87,** 386–393
12. Okamatsu, Y., Kim, D., Battaglino, R., Sasaki, H., Spate, U., and Stashenko, P. (2004) *J. Immunol.* **173,** 2084–2090
13. Kominsky, S. L., Abdelmagid, S. M., Doucet, M., Brady, K., and Weber, K. L. (2008) *Cancer Res.* **68,** 1261–1266
14. Binder, N. B., Niederreiter, B., Hoffmann, O., Stange, R., Pap, T., Stulnig, T. M., Mack, M., Erben, R. G., Smolen, J. S., and Redlich, K. (2009) *Nat. Med.* **15,** 417–424
15. Gao, J. L., Wynn, T. A., Chang, Y., Lee, E. J., Broxmeyer, H. E., Cooper, S., Tiffany, H. L., Westphal, H., Kwon-Chung, J., and Murphy, P. M. (1997) *J. Exp. Med.* **185,** 1959–1968
16. Doi, M., Nagano, A., and Nakamura, Y. (2002) *Biochem. Biophys. Res. Commun.* **290,** 381–390
17. Hoshino, A., Kawamura, Y. I., Yasuhara, M., Toyama-Sorimachi, N., Yamamoto, K., Matsukawa, A., Lira, S. A., and Dohi, T. (2007) *J. Immunol.* **178,** 5296–5304
18. Ito, M., Ikeda, K., Nishiguchi, M., Shindo, H., Uetani, M., Hosoi, T., and Orimo, H. (2005) *J. Bone Miner. Res.* **20,** 1828–1836
19. Parfitt, A. M., Drezner, M. K., Glorieux, F. H., Kanis, J. A., Malluche, H., Meunier, P. J., Ott, S. M., and Recker, R. R. (1987) *J. Bone Miner. Res.* **2,** 595–610
20. Liotta, L. A., and Stetler-Stevenson, W. G. (1990) *Semin. Cancer Biol.* **1,** 99–106
21. Gogly, B., Groult, N., Hornebeck, W., Godeau, G., and Pellat, B. (1998) *Anal. Biochem.* **255,** 211–216
22. Wilson, M. J., Strasser, M., Vogel, M. M., and Sinha, A. A. (1991) *Biol. Reprod.* **44,** 776–785
23. Komori, T., Yagi, H., Nomura, S., Yamaguchi, A., Sasaki, K., Deguchi, K., Shimizu, Y., Bronson, R. T., Gao, Y. H., Inada, M., Sato, M., Okamoto, R., Kitamura, Y., Yoshiki, S., and Kishimoto, T. (1997) *Cell* **89,** 755–764
24. Ducy, P., Zhang, R., Geoffroy, V., Ridall, A. L., and Karsenty, G. (1997) *Cell* **89,** 747–754

25. Liu, W., Toyosawa, S., Furuichi, T., Kanatani, N., Yoshida, C., Liu, Y., Himeno, M., Narai, S., Yamaguchi, A., and Komori, T. (2001) *J. Cell Biol.* **155,** 157–166
26. Delmas, P. D. (1993) *J. Bone Miner. Res.* **8,** Suppl. 2, S549–S555
27. Takahashi, M., Kushida, K., Hoshino, H., Ohishi, T., and Inoue, T. (1997) *J. Endocrinol. Invest* **20,** 112–117
28. Schneider, D. L., and Barrett-Connor, E. L. (1997) *Arch. Intern. Med.* **157,** 1241–1245
29. Arai, F., Miyamoto, T., Ohneda, O., Inada, T., Sudo, T., Brasel, K., Miyata, T., Anderson, D. M., and Suda, T. (1999) *J. Exp. Med.* **190,** 1741–1754
30. Saitoh, Y., Koizumi, K., Sakurai, H., Minami, T., and Saiki, I. (2007) *Biochem. Biophys. Res. Commun.* **364,** 417–422
31. Abe, M., Hiura, K., Wilde, J., Moriyama, K., Hashimoto, T., Ozaki, S., Wakatsuki, S., Kosaka, M., Kido, S., Inoue, D., and Matsumoto, T. (2002) *Blood* **100,** 2195–2202
32. Chintalacharuvu, S. R., Wang, J. X., Giaconia, J. M., and Venkataraman, C. (2005) *Immunol. Lett.* **100,** 202–204
33. Kanatani, N., Fujita, T., Fukuyama, R., Liu, W., Yoshida, C. A., Moriishi, T., Yamana, K., Miyazaki, T., Toyosawa, S., and Komori, T. (2006) *Dev. Biol.* **296,** 48–61
34. Sakai, N., Wada, T., Furuichi, K., Shimizu, K., Kokubo, S., Hara, A., Yamahana, J., Okumura, T., Matsushima, K., Yokoyama, H., and Kaneko, S. (2006) *J. Leukoc. Biol.* **79,** 555–563
35. Furuichi, K., Gao, J. L., Horuk, R., Wada, T., Kaneko, S., and Murphy, P. M. (2008) *J. Immunol.* **181,** 8670–8676
36. Ma, B., Zhu, Z., Homer, R. J., Gerard, C., Strieter, R., and Elias, J. A. (2004) *J. Immunol.* **172,** 1872–1881
37. Shang, X., Qiu, B., Frait, K. A., Hu, J. S., Sonstein, J., Curtis, J. L., Lu, B., Gerard, C., and Chensue, S. W. (2000) *Am. J. Pathol.* **157,** 2055–2063
38. Anders, H. J., Frink, M., Linde, Y., Banas, B., Wörnle, M., Cohen, C. D., Vielhauer, V., Nelson, P. J., Gröne, H. J., and Schlöndorff, D. (2003) *J. Immunol.* **170,** 5658–5666
39. Coates, P. T., Colvin, B. L., Ranganathan, A., Duncan, F. J., Lan, Y. Y., Shufesky, W. J., Zahorchak, A. F., Morelli, A. E., and Thomson, A. W. (2004) *Kidney Int.* **66,** 1907–1917
40. Ishii, M., Egen, J. G., Klauschen, F., Meier-Schellersheim, M., Saeki, Y., Vacher, J., Proia, R. L., and Germain, R. N. (2009) *Nature* **458,** 524–528
41. Matsuo, K., and Irie, N. (2008) *Arch. Biochem. Biophys.* **473,** 201–209
42. Kitazawa, R., Mori, K., Yamaguchi, A., Kondo, T., and Kitazawa, S. (2008) *J. Cell Biochem.* **105,** 1289–1297
43. Murphy, P. M., Baggiolini, M., Charo, I. F., Hébert, C. A., Horuk, R., Matsushima, K., Miller, L. H., Oppenheim, J. J., and Power, C. A. (2000) *Pharmacol. Rev.* **52,** 145–176
44. Terashima, Y., Onai, N., Murai, M., Enomoto, M., Poonpiriya, V., Hamada, T., Motomura, K., Suwa, M., Ezaki, T., Haga, T., Kanegasaki, S., and Matsushima, K. (2005) *Nat. Immunol.* **6,** 827–835
45. Sato, K., Suematsu, A., Okamoto, K., Yamaguchi, A., Morishita, Y., Kadono, Y., Tanaka, S., Kodama, T., Akira, S., Iwakura, Y., Cua, D. J., and Takayanagi, H. (2006) *J. Exp. Med.* **203,** 2673–2682
46. Votta, B. J., White, J. R., Dodds, R. A., James, I. E., Connor, J. R., Lee-Rykaczewski, E., Eichman, C. F., Kumar, S., Lark, M. W., and Gowen, M. (2000) *J. Cell Physiol.* **183,** 196–207
47. Rioja, I., Hughes, F. J., Sharp, C. H., Warnock, L. C., Montgomery, D. S., Akil, M., Wilson, A. G., Binks, M. H., and Dickson, M. C. (2008) *Arthritis Rheum* **58,** 2257–2267

J Bone Miner Metab (2010) 28:641–649
DOI 10.1007/s00774-010-0181-4

ORIGINAL ARTICLE

Repetition of continuous PTH treatments followed by periodic withdrawals exerts anabolic effects on rat bone

Masaya Etoh · Akira Yamaguchi

Received: 10 January 2010 / Accepted: 7 March 2010 / Published online: 15 April 2010

Abstract Various animal experiments and human studies have shown that intermittent injections of parathyroid hormone (PTH) exert anabolic effects on bone, whereas continuous PTH treatment decreases the bone mass and causes hypercalcemia in animals. However, limited data are available with regard to the effects of a repetitive regimen of continuous treatments of PTH followed by periodic withdrawals on the bone metabolism. We investigated the effects of this regimen by comparing the findings of intermittent and continuous PTH treatments in rats. Infusions of PTH for 24 h followed by 6-day withdrawal periods from PTH transiently increased the serum calcium levels on day 1, but these levels were within the normocalcemic range. The repetition of 4 cycles of continuous PTH infusions followed by PTH withdrawals as well as intermittent PTH treatment increased the trabecular bone thickness, osteoblast surface, and bone formation rate. Continuous PTH infusions followed by PTH withdrawals also increased the cortical thickness of the femoral diaphysis and the osteoid volume in trabecular bones, whereas the continuous treatment failed to induce these changes. These findings suggest that continuous PTH treatment followed by PTH withdrawal is a potential regimen that can induce the anabolic effects of PTH in bone metabolism without inducing hypercalcemia.

Keywords Parathyroid hormone · Bone mineral density · Mechanical properties · Intermittent treatment · Continuous treatment

M. Etoh · A. Yamaguchi (✉)
Section of Oral Pathology, Tokyo Medical and Dental University Graduate School, 1-5-45 Yushima, Bunkyo-ku, Tokyo 113-8549, Japan
e-mail: akira.mpa@tmd.ac.jp

A. Yamaguchi
Global Center of Excellence Program, International Research Center for Molecular Science in Tooth and Bone Diseases, Tokyo Medical and Dental University, Tokyo, Japan

Introduction

Parathyroid hormone (PTH) regulates bone remodeling through its action on bone formation as well as bone resorption. Studies using serum biochemical markers and bone histomorphometric analysis have shown that both intermittent and continuous PTH treatments stimulate bone turnover in trabecular and cortical bones [1–3].

Intermittent PTH treatment, which is administered via daily injections or daily short-time infusions, increases trabecular and cortical bone mass in not only normal rats [4, 5], but also ovariectomized rats [6]. These studies revealed that the optimal exposure time and frequency required to induce anabolic effects through intermittent PTH treatment are 1 h and 1–3 times per day, respectively [5, 7]. Many human studies with intermittent PTH injections also showed apparent anabolic effects on bone mass and prevention of bone fractures [8]. Although the recommended dose regimen of Forteo, a potent Food and Drug Administration (FDA)-approved drug for the treatment of osteoporosis, is once a day by self-administered injections, compliance with this regimen is moderate because of high cost and adverse effects such as pain at the injection sites [9].

To avoid these adverse events, new suitable therapeutic regimens are required. One possible regimen is extension of the interval of intermittent PTH injection, but it has not been

clearly understood whether the elongated injection interval of PTH treatment induces similar anabolic action with daily PTH injection under the same total dose of PTH [10]. A possible alternative regimen is short-term continuous PTH treatment associated with a long-term withdrawal period. In this context, continuous PTH exposure by using osmotic pumps in rats results in hypercalcemia and decreased bone mass. However, various parameters of PTH treatment regimens, such as the exposure time in the continuous treatment and periodic withdrawals, have not been well documented. If continuous PTH treatment in combination with a relatively long-term withdrawal period is found to induce an anabolic effect in bones, an alternative clinical dosing regimen can be established on the basis of these findings. For example, daily subcutaneous injections of PTH could be replaced by a weekly injection of sustained controlled release PTH. This regimen can decrease the number of injections and may prevent patients from discontinuing the treatment. Furthermore, sustained pharmacokinetics may be more acceptable in the oral administration of PTH-mimicking peptides by using a drug delivery system [11].

In the present study, we conducted experiments to investigate a new therapeutic regimen of PTH administration that induces anabolic effects on bone metabolism that are comparable with those of classical intermittent PTH administration. We compared the effects of three regimens: intermittent PTH treatment, continuous PTH treatment, and repetition of continuous PTH treatments followed by periodic withdrawals. Here, we show that continuous PTH administration with periodic withdrawals exerts an anabolic effect on the bone metabolism in rats.

Materials and methods

Chemicals

Synthetic human PTH (1–34) was purchased from the Peptide Institute (Osaka, Japan) and prepared at an appropriate dose in a vehicle (10 mM acetic acid, 2% heat-inactivated rat serum in sterile PBS). Calcein was purchased from Sigma (St. Louis, MO).

Animals

Nine-week-old female Sprague-Dawley rats (Charles River, Kanagawa, Japan) were used in this study. They were maintained under 12:12 h light/dark cycles with unrestricted access to tap water and a standard diet containing 1.2% Ca, 0.9% P, 22% protein, and 6.2 IU vitamin D3 per gram (CRF-1; Oriental Yeast, Tokyo, Japan). The animals were allowed to acclimatize for 12 days before the start of the experiment. The animal studies were performed in compliance with the standards mentioned in the Care and Management of Laboratory Animals and Relief of Pain (Notice no. 88 of the Japanese Ministry of Environment, 2006).

Experimental groups

As shown in Table 1, the rats were divided into three groups (intermittent PTH treatment group, continuous PTH treatment group, and continuous PTH treatment with withdrawal group) with equal body weight distributions. Intermittent PTH treatments were administered by subcutaneous injections of PTH with a total dose of 40 μg/kg/week. This group comprised three regimens: PTH injection (40 μg/kg) once a week (I×1-PTH), PTH injection (13.3 μg/kg) 3 times a week (I×3-PTH), and vehicle injection 3 times a week (I-CON). Continuous PTH treatment was conducted by subcutaneous implantation of Alzet micro-osmotic pumps (Model 1007D; Durect Corp., CA), which constantly deliver a fluid for 7 days. The Alzet pumps were aseptically filled with appropriate amounts of PTH or the vehicle, and the pumps were replaced every week. This group also comprised three regimens. The first regimen was continuous PTH treatment with a dose of 0.24 μg/kg/0.5 μl/h (C40-PTH), in which the total dose of PTH supplement (40 μg/kg/week) was administered. The second regimen was continuous PTH treatment with a dose of 1.67 μg/kg/0.5 μl/h (C280-PTH), in which the total dose of PTH 280 μg/kg/week was administered. This regimen was used as a positive control for PTH-induced hypercalcemia. The third regimen of this group was continuous treatment with the vehicle (C-CON). Continuous PTH treatment with withdrawal (PTH-WD) was conducted by continuous PTH treatment for 24 h through the subcutaneously implanted Alzet micro-osmotic pumps (Model

Table 1 Experimental design

Experimental group	Total dose (μg/kg/week)	Abbreviations
Intermittent		
Control	0	I-CON
PTH 40 μg/kg × 1 injection/week	40	I×1-PTH
PTH 13.3 μg/kg × 3 injections/week	40	I×3-PTH
Continuous		
Control	0	C-CON
PTH 40 μg/kg/week	40	C40-PTH
PTH 280 μg/kg/week	280	C280-PTH
Continuous-withdrawal		
Control	0	CON-WD
PTH 40 μg/kg/24 h 6-day withdrawal	40	PTH-WD